To be published as a Chapter in "Practical X-Ray Spectroscopy", Dr. L. S. Birks, eds., Marcel Dekher Inc.

LBL-5354

ENERGY DISPERSION

Joseph M. Jaklevic and Fred S. Goulding

May 1976

Prepared for the U. S. Energy Research and Development Administration under Contract W-7405-ENG-48

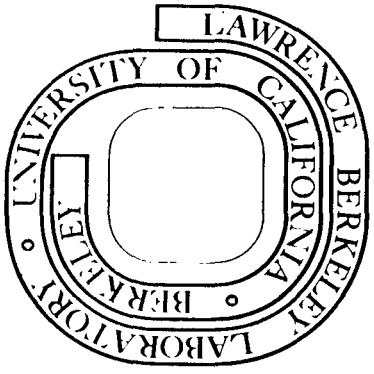

LBL-5354

DISCLAIMER

LBL-5354

Editor: Dr. L. S. Birks

CHAPTER 3

ENERGY DISPERSION

Joseph M. Jaklevic and Fred S. Goulding

Department of Electronics Engineering
Lawrence Berkeley Laboratory
University of California
Berkeley, California 94720 U.S.A.

May 1976

CHAPTER TABLE OF CONTENTS

CHAPTER 3

ENERGY DISPERSION

Chapter 3

ENERGY DISPERSION*

Joseph M. Jaklevic and Fred S. Goulding

Department of Electronics Engineering
Lawrence Berkeley Laboratory
University of California
Berkeley, California 94720 U.S.A.

I. INTRODUCTION

In energy-dispersive X-ray fluorescence spectrometry identification of fluorescence radiation is performed using detectors which directly measure the X-ray energy. Such detectors normally operate by measuring the consequence of interactions of the incident X rays in the detector medium. In the simplest case, an electron is ejected from an atom in the detector by photoelectric absorption of the incident X ray. The final result is then produced by the slowing down of this primary electron resulting in showers of electron-ion pairs in the case of a proportional counter, optical excitations in the case of a scintillation detector, or showers of electron-hole pairs in a semiconductor detector. The output from the detector is the integral of such effects which for our present purposes we can regard as proportional to the energy of the original incident X ray. This method is in contrast to wavelength dispersion in which the Bragg reflecting properties of a crystal are used to disperse X rays at different reflection angles according to their wavelength.

Although energy-dispersive detectors generally exhibit poorer energy resolution than wavelength-dispersive methods, they are capable of simultaneous detection of a wide range of X-ray energies and have inherently higher detection efficiencies. In order to operate effectively as a detector for X-ray fluorescence applications the energy resolution must be adequate to resolve the characteristic X rays of interest from interfering lines and background. The recent development of semiconductor detectors with their excellent

* This work was performed under auspices of the United States Energy Research and Development Administration.

energy resolution has made energy-dispersive X-ray fluorescence analysis a powerful analytical tool whose applications are rapidly expanding. Spectrographic applications of the other types of energy-dispersive detector are now limited to special cases where certain features of semiconductor detectors are not acceptable, such as in space where cryogenic cooling is difficult.

Most semiconductor detectors used for X-ray analysis consist of a single crystal of either silicon or germanium, typically 1 cm or less in diameter and 0.3 to 1 cm thick. Free charge produced by the interaction of each incident X ray in the detector is collected and accurately measured. To obtain the energy resolution required for X-ray spectroscopy it is necessary to operate the device at a low temperature and a liquid nitrogen cryostat is normally used to maintain the detector at 77°K (-196°C).

Figures 1(a) and 1(b) illustrate energy resolution capabilities as a function of X-ray energy over the range of interest in fluorescence spectroscopy. The upper figure shows the variation $\Delta E/E$ with energy for typical semiconductor detectors and proportional counters. Scintillation detectors would exhibit still poorer energy resolution. Also shown is the performance of a typical wavelength dispersive crystal spectrometer illustrating the improved energy resolution achieved by this method in the lower energy range. The lower figure shows ΔE (FWHM) for a typical state-of-the art lithium-drifted silicon detector spectrometer operating at 77°K. The energy resolution at low energies (120 eV in Fig. 1(b)) is determined by electronic noise. Small lithium-drifted or high-purity germanium detectors exhibit comparable resolution.

The dominant importance of good energy resolution in analytical X-ray spectroscopy is illustrated in Fig. 2(a) which shows the energies of the characteristic K X rays of the low Z elements and the L X rays of the heavy elements. Figure 2(b) shows the separations of the K_α lines of adjacent elements as Z changes, and also the separation of the K_α line of an element from the K_β line of the next lower Z element. When those results are compared with the energy resolution curve of Fig. 2(a), it becomes obvious that separation of the K_α lines of adjacent elements is impossible for the very light elements ($Z < 6$); even more important, interference between the K_β line of an element and the K_α line of the next higher Z element is serious for much

higher values of Z. Fortunately, computer analysis of the whole spectrum, taking into account the known X-ray line structures of the various elements, can accommodate a reasonable level of such interference. These techniques are also necessary to overcome interferences between the L and M lines of heavy elements and the K lines of light elements. These problems are reduced by using detector systems with improved energy resolution.

Since the excellent energy resolution of wavelength-dispersive system avoids many of these interference, it would seem that there would be little use for energy-dispersive systems. However, the need for precise collimation in wavelength-dispersive systems results in a greatly reduced efficiency for X-ray detection with the result that the analytical sensitivity for the detection of elements is often comparable for the two methods [1]. The simultaneous multielement capability of energy-dispersive systems therefore gives them an important role in X-ray analysis.

II. BASIC METHODS

The basic elements of an energy-dispersive X-ray fluorescence spectrometer are illustrated in Fig. 3. Excitation can be any form of radiation capable of producing vacancies in the inner shells of the atoms of interest in the sample. These vacancies are then filled by transitions of electrons from higher-energy atomic orbitals resulting in the emission of characteristic X rays. Measurement of the energies and intensities of these X rays is the basis of a X ray fluorescence spectroscopy. A competing process whereby vacancies fill involves the Auger effect in which deexcitation proceeds by emission of an outer shell electron instead of an X-ray photon. This process becomes more likely than X-ray emission for the light elements where the fraction of vacancies producing X-ray emission (defined as the fluorescence yield ω) may be less than 10% [2].

The detector shown in Fig. 3 is normally collimated to accept X rays which originate at the sample and have sufficient energy to penetrate the thin entrance window to the detector. The observed energy spectrum contains not only the characteristic X rays of interest but also those from other

elements in the sample. An additional background caused by other types of interactions such as scattering of the excitation radiation from the sample can be observed. The magnitude and spectral shape of the background depends on the type and energy of the excitation and on the composition of the sample.

Various types of exciting radiation may be employed; the choice between them depends both on fundamental physical processes, which determine the ultimate performance potential in a given application, and on very practical factors such as cost and availability. Performance factors which must be considered include such matters as background, which establishes the limit of detectability and sensitivity, the accuracy of the quantitative information obtained and the range of elements over which optimum sensitivity is achieved. The available options for excitation are electrons, positive ions and photons (i.e., X rays or gamma rays). The relative cross sections for inner-shell vacancy production for the three methods are similar enough that the choice between them is usually based on other factors.

The use of electrons for excitation has the advantage that they can be conveniently generated in large quantities and that their energy and intensity can easily be regulated. They have the disadvantages that the sample must be enclosed in the same vacuum as the source and that the ratio of fluorescent signal to background is relatively poor due to the large amount of continuum Bremsstrahlung radiation produced in the sample. This radiation is caused by the decelerations which electrons undergo as they interact with the positively charged nuclei in the sample producing a continuous X-ray spectrum with a maximum energy equal to that of the incident electrons. The portion of this radiation seen by the detector sets a fluorescence analysis detection limit considerably higher than when using other excitation methods. However, the ability to focus electrons into precisely controlled beams of sub-micron size has led to extensive applications of energy-dispersive detectors in electron microprobe analysis and in scanning electron microscopes. These applications are discussed in Chapter 4. Other uses of electron-excited X-ray fluorescence are described in Chapter 7.

Since positive ions are much more massive than electrons they produce less Bremsstrahlung radiation, and background in the fluorescence spectrum is a much smaller problem. Although not as convenient as electrons to generate, proton and alpha particle beams are available at nuclear research

accelerators with the result that much recent work has been done in this area. As with electrons, samples must be contained in a vacuum shared with the particle accelerator. The basic limit to the detectability of this method is the continuum Bremsstrahlung radiation produced by energetic secondary electrons resulting from collisions of the incident ions with electrons in the sample. The resulting radiation background has an end-point energy which is directly related to the energy of the original ion beam. Consequently optimum sensitivities for most analytical applications are achieved with beam energies below 16 MeV for alpha particles and 3 MeV for protons corresponding to a Bremsstrahlung background end-point energy of 6 to 8 keV. Excellent detection limits have been achieved under these conditions particularly in situations where the thickness and size of the sample is optimum for this type of analysis [3]. A more complete discussion of the capabilities of charged-particle excitation analysis is presented in Chapter 7.

Photon-excited X-ray fluorescence analysis will be discussed in more detail in the present chapter. This approach has been extensively used and appears to be the most useful for general analytical applications, partly based on excellent performance, but also because it is very convenient to use compared with other excitation methods.

In passing through matter, photons do not undergo continuous energy loss processes as do charged particles. The absorption obeys an exponential attenuation law:

$$I = I_o e^{-\mu\rho x} \qquad (1)$$

where I_o is the initial intensity of the beam in photons/sec,
ρ is the density of the material in gm/cm^3,
I is the intensity transmitted through a thickness x(cm),
μ is the mass attenuation coefficient expressed in units of cm^2/gm.

The attenuation coefficient μ can be broken down into components associated with the various absorption processes. In considering fluorescence, the portion associated with photoelectric absorption is the important part as far as

excitation of characteristic X ray is concerned. The photoelectric absorption cross-section is zero for incident photon energies less than the binding energy of the particular atomic shell of a given element and jumps to a maximum immediately above that energy. As the energy is increased still further, the cross section decreases as approximately $E^{-3.5}$. This is an important factor in the choice of excitation energy since the sensitivity for detection is greatest for those elements whose absorption edges are just below the incident photon energy. Figure 4 is a plot of the relative photoelectric cross-section per individual atom as a function of energy for several elements [4].

Photons also interact by scattering from the sample so, in the general case, μ is the sum of the scattering and absorption components. Furthermore, since the typical sample of interest in fluorescence spectroscopy contains atoms of many elements, the quantity μ must be replaced by a summation over all the elements and their relative concentrations:

$$\mu\rho \rightarrow \Sigma_i \, \mu_i \, \rho_i \qquad (2)$$

where the subscript i refers to element i in the sample.

The relative magnitude of the various unwanted scattering and absorption processes as compared with the desired vacancy production by photoelectric absorption determines the sensitivity for photon-excited fluorescence analysis. If the sample contains mostly elements of high atomic number, photoelectric absorption is dominant and the concentrations are determined by the relative magnitudes of the fluorescence peaks in the spectrum. On the other hand, if the elements of interest are contained in a low-Z matrix, the background produced by scattering processes affects the sensitivity too.

The characteristics of photon-induced fluorescence and detection limits are best discussed in terms of a hypothetical fluorescence spectrum. To simplify the problem, excitation will be considered to be in the form of monoenergetic photons and the sample will be assumed to be sufficiently thin that the probability of multiple interactions is small. Extensions to broad energy range excitation and to thicker samples involves obvious integrations over the

incident spectral distribution and over the sample thickness. The three modes of interaction of importance for photons in the energy range of interest are Rayleigh scattering, Compton scattering and photoelectric absorption. In Rayleigh scattering an incident photon interacts with a tightly bound atomic electron and thereby is elastically scattered with no loss of energy. In Compton scattering the interaction takes place with a loosely bound electron resulting in an energy loss in the scattered photon governed by the well known Compton equation of atomic physics. Figure 5 shows the resulting energy loss as a function of scattering angle and incident photon energy. The photons scattered by either of these processes can reach the detector and contribute unwanted counts in the spectrum.

Figure 6 shows the idealized spectrum produced by a semiconductor detector system in a fluorescence measurement using monoenergetic photon excitation. The plot represents the number of events analyzed by the detector as a function of the size of the pulse from the detector. The highest energy peak in the spectrum occurs at the energy of the incident excitation and is due to X rays that Rayleigh scatter from the sample into the detector. The broad peak at slightly lower energy is due to the inelastic Compton scattering. The width of this peak reflects the spread of angles over which the photons are scattered and the corresponding energy losses according to the Compton relationship. The low-energy continuous distribution is due to Compton scattering in the detector whereby high-energy X rays reaching it are scattered out leaving only that fraction of their energy which had been imparted to electrons in the detector. Fluorescence signals are represented by the small peaks occurring at energies well below the high-energy scatter peaks. The magnitude of each peak is dependent upon the concentration of a particular element in the sample and on the relative cross section for the K or L shell ionization of the element as shown in Fig. 4. Background beneath the peaks is due to a number of complex interactions by which the high-energy scattered X rays can produce a continuum of pulse amplitudes in the detector. These can then be the result of poor charge collection in the detector or they can arise from the Bremsstrahlung produced in the sample by slowing down of secondary electrons. Both these effects are serious in trace element applications. For the purpose of the present discussion it is sufficient to observe that the detection limit is set by this background which, in turn, is proportional to the total scattered intensity.

The idealized spectrum of Fig. 6 represents the case of trace elements in a low atomic number matrix such as hydrocarbons. In this simplified example, most of the atoms in the sample are of low Z elements that contribute for most of the scattered X-ray intensity. If the average atomic number of the matrix is increased, the relative magnitude of Rayleigh vs. Compton scattering changes since the approximate Z^2 dependence of elastic scattering predominates over the $\propto Z$ dependence of the Compton effect. As the average atomic number is increased photoelectric absorption and the resulting fluorescence of the atoms in the matrix become important; analysis of the spectrum is then complicated by interelement absorption and enhancement effects. Since the heavier elements then absorb a significant fraction of the beam photoelectrically, the fluorescence spectrum consists predominantly of the X rays emitted by atoms of these elements. If the energies of these intense fluorescent X rays are above the absorption edge of other constituents in the sample, they can be reabsorbed and contribute to an enhancement of the X ray yield of the lower Z elements. Both the absorption and enhancement effects contribute to a nonlinear relationship between the concentration and the measured X ray intensity. These problems are well known in X-ray spectroscopy of specimens such as alloys and are discussed elsewhere in this book.

Practical X ray sources often do not provide perfectly monochromatic excitation. A close approximation can be achieved by using characteristic X rays generated directly by a X-ray tube or by a radioactive source, or indirectly by a secondary fluorescence system in which the X rays from the primary source fluoresce a secondary pure-element target. The interpretation of the spectrum is then as discussed above. In some cases it proves more convenient to use a continuous Bremsstrahlung spectrum for excitation. The spectrum in the detector is then a superposition of spectra corresponding to each energy in the continuum, (i.e. it is an integral over the continuous excitation distribution function). Since the scattered radiation extends over the whole spectrum, the background below the characteristic X-rays is higher than with monochromatic excitation. However, detectability may be less important in some cases than the fact that the wideband excitation gives a more uniform sensitivity over a wide range of elements.

The methods of photon excitation illustrated in Fig. 7 include radioisotope and X-ray tube sources used in direct or secondary fluorescence configurations. Direct excitation can employ either a broadband or monochromatic

radiation. The principal difference between radioisotope sources and X-ray tubes is the large difference in available intensity. The radiation hazard associated with the use, handling and storage of a very active source, imposes a practical upper limit of 100 millicuries (1 Curie = 3.7×10^{10} disintegrations/sec), whereas an X-ray tube, which need only be turned on when required, can easily be equivalent to 10 to 1000 Curies. To achieve reasonably detectability using radioactive sources the total sample mass should be large and long analysis times must be tolerated. Monochromatic radioisotope sources are generally used although continuous sources are also available. Radioisotope sources are used mainly because of their low cost, small size and simplicity and can be used successfully where the analysis of large numbers of samples is not required. Apart from the lack of adequate intensities, another disadvantage arises from the relatively small number of available isotopes. Table 1 is a list of radioisotope sources commonly used for X-ray fluorescence; most are commercially available in packages convenient for either direct or secondary fluorescence excitation. A more complete description of possible radioisotope options is given in Ref. 5.

X-ray tubes provide controllable photon energy and intensity but are more costly than radioisotopes and require a high-voltage power supply and associated controller. Therefore they are used in large-scale analytical programs where the speed of analysis more than compensates for the initial cost. The direct output of a typical X-ray tube consists of the electron-excited characteristic X rays of the anode material together with a continuous Bremsstrahlung spectrum. The output can be filtered with an appropriate absorber, normally the same material as the anode, to provide a source predominately composed of the characteristic X rays of the anode material. A better method of creating monochromatic radiation employs the secondary target system shown in Fig. 7. The spectral output in this case has much less continuum radiation but at a considerable sacrifice in intensity compared with the case of direct excitation.

The use of monochromatic X-ray excitation results in a very high sensitivity for detection of elements with absorption edges slightly lower in energy than the excitation, and a decreasing sensitivity for lower Z elements. For adequate coverage of a wide range of elements the sample must

be exposed sequentially to a number of excitation energies. This is in contrast to the case of continuous excitation where the detection sensitivity is poorer but a uniform coverage of a wide range of elements is achieved in one exposure.

One set of excitation energies suitable for analysis of a wide range of elements corresponds to the characteristic X rays of elements Cu, Mo and Tb at 10, 20 and 44 keV respectively. Figure 8 is a plot of the calculated relative fluorescence excitation probabilities as a function of Z for this set. The rapidly decreasing values for low Z elements results from the decrease in fluorescence yield (i.e. a larger probability of vacancy filling being accompanied by Auger electron emission). This choice of elements for excitation is not unique and optimum detection of specific elements may require intermediate excitation energies. A practical restriction is that the secondary target should be able to be produced in a form appropriate for the geometry employed and in a chemical state not easily damaged by the X-ray radiation flux. The choice of Cu, Mo and Tb is dictated to a large extent by their availability as stable metallic foils.

R. Giauque, et al have reported on the single-element detectable limits obtained in a series of different types of samples using Mo K X ray for excitation [6]. Using a criteria for minimum detectable limit defined as a signal 3σ above background, and a counting time of 1000 secs, measured limits were below 1 ppm for elements with $24 < Z < 37$ and also for Hg and Pb contained in a biological sample (i.e. a hydrocarbon matrix). A detectable limit of 1 ppm was observed for elements in the Cd region using Tb K X-ray excitation. Russ has reported detection limits in the 1 to 10 ppm range in aqueous solutions over the same region using continuous Bremsstrahlung radiation and comparable counting times [7]. Similar detectability can be achieved using radioisotope excitation but counting times of the order of 10 to 100 times longer must be used.

Commercial X-ray fluorescence equipment manufacturers produce systems based on the various options discussed above. Since each approach has particular merits for a given class of applications, no simple conclusion regarding the superiority of any approach can be given.

A discussion of X-ray excitation sources would not be complete without mention of some other aspects of the generation of X rays which may prove useful for certain applications. Recent papers have discussed the benefits

of polarized X-ray beams and means of generating them [8,9]. The advantage of polarized excitation is that no scattering is observed parallel to the direction of polarization of the incident radiation, resulting in a drastically reduced background. However, current techniques for generating polarized X-ray beams involve multiple scattering with a prohibitive reduction in the usable intensity. Alternative polarized X-ray sources, such as the synchrotron radiation produced by very high-energy electron storage rings offer high intensities but are not available for general use.

III. INSTRUMENTAL CONSIDERATIONS

A. Detectors

As noted earlier, the principal advantage of semiconductor detectors over others is their improved energy resolution. Secondary factors which influence their application to a given problem include efficiency, background characteristics and counting-rate capabilities. In the following paragraphs the general feature of semiconductor-detector spectrometers will be discussed.

Figure 9 is a cutaway view of a typical lithium drifted silicon X-ray detector. The device is known as a p-i-n structure referring to the p-type contact on the entry side, the intrinsic active volume, and the lithium-diffused n contact. The active volume consists of a region in which the donor lithium has been drifted under the influence of an electric field to precisely compensate p-type impurities in the original silicon. When reverse bias is applied to the device the drifted region acts as an insulator with an electric field throughout its volume. At liquid nitrogen temperature, it exhibits very low leakage current, so signals produced by radiation-induced ionization are easily detected. Germanium detectors may also be used in some X-ray spectrometers. The lithium-drifting process has been employed in the past in germanium as well as silicon, but high-purity germanium detectors are now available. Since no lithium compensation is present these detectors can, when absolutely necessary, be temperature cycled to room temperature--unlike

lithium-drifted germanium detectors. Since the mobility of lithium in silicon is much lower than in germanium, lithium-drifted silicon detectors can also be temperature cycled.

The p-type surface barrier contact (a metal evaporation) is made very thin; entrance windows below 0.2 μm are typical. The intrinsic region is the sensitive volume of the detector where photoelectrons are produced and lose energy producing ionization in the form of free holes and electrons. These free charges are swept away by the applied bias and collected. Since a well defined average energy is required to produce an electron-hole pair in a particular semiconductor material, the total number of charges produced is directly proportional to the energy of the absorbed X ray (assuming total X ray absorption). In an ideal detector the total charge is completely collected for each detector event and the response of the system to monochromatic photons is a single peak with zero counts elsewhere in the spectrum. However, observed spectra obtained with real semiconductor detectors exhibit a continuous background extending from zero energy to that of the principal peak. Investigations of the nature of this background have established that its origin is the distortion of internal electric fields caused by the detector surfaces present in most geometries [10]. Figure 10(a) shows a cross section of a typical detector. The shaded portions indicate areas in which the internal field lines do not terminate at the electrical contact formed by the metal surface barrier but, instead, terminate on the ill defined surfaces. Events occurring within this region experience incomplete collection of the charge signal resulting in a smaller signal than should be produced. To the extent that such events are continuously distributed up to the amplitude corresponding to the full energy peak, they account for much of the observed continuum background.

The magnitude of the continuum relative to the peak can be reduced by using a larger detector and collimated the incoming radiation to avoid the shaded regions. Another approach is to use the guard-ring detector illustrated in Fig. 10(b). Here, an addition annular contact or guard ring is added on the lithium-diffused side and maintained at the same dc potential as the central region. The signal is taken from the central area while the outer ring serves to maintain uniform internal field lines in the detector.

Such guard-ring detectors show greatly reduced background. Further reduction can be achieved by extracting a signal from the guard ring and, if an event occurs sufficiently close to the edge of the sensitive region that a portion of the charge is collected in the guard ring, the coincident signal in the active region is rejected. This is termed the 'guard-ring reject' method.

Assuming that the appropriate measures are taken to reduce such detector artifacts as these then the fundamental limit in detector background below the principal peak is established by the escape of secondary particles or photons from the detector surfaces. Photoelectric absorption of an X ray in the detector ejects an electron from one of the shells of Si or Ge atoms creating a vacancy which subsequently fills with accompanying emission of Si or Ge characteristic X rays or an Auger electron. To produce a 'full energy' signal, the whole energy of the initial photoelectron and that of the secondary radiation produced when the Si or Ge atom deexcites must be absorbed in the sensitive region of the detector. Any loss of energy will cause a signal smaller than desired resulting in detector background. This type of detector background is fundamental depending only on the characteristics of the detector material and on its geometry. It should be noted that even in the ideal case where continuous background due to detector effect could be reduced to zero there would still be significant background contribution due to Bremsstrahlung produced in the sample by the electrons ejected from atoms in the sample.

The escape of a characteristic X ray of the detector material subtracts a definite energy from an event and such events produce discrete 'escape' peaks in the background distribution at energies slightly below the main peaks. In the case of Si the K-escape causes a peak at an energy 1.74 keV less than the full energy peak. Due to the large penetration depth of X rays in Si and the small fluorescence yield of Si vacancies, these peaks are important for photon energies below 6 keV and cannot achieve a size of more than 2% of the full energy peak. In Ge K-escape peaks occur at an energy of 9.87 or 11.0 keV below the main peak depending whether the K_α or K_β X rays escape. Due to the large fluorescence yield in Ge and the penetration of these high-energy X rays, these peaks can be as large as 20% of the full energy peak

intensity. Since the energy of these peaks occurs in a very awkward range from the point of view of fluorescence analysis, Ge detectors find only limited applications here.

The efficiency of Ge detectors is much higher than that for Si detectors at high energies due to the Z^5 dependence of photoelectric cross sections. Figure 11 shows the efficiency variation of various detectors with energy. Note that the Ge detector efficiency changes rapidly in the 10 keV region near the K-shell absorption edges. In practical systems the fall off in efficiency at low energies is set by the thickness of Be window on the cryostat vacuum enclosure. The curves of Fig. 11 are for a 25 μm window but Be windows as thin as 7 μm can be fabricated where good low-energy efficiency is essential. Air absorption is also important in such systems so helium or vacuum paths are provided between the sample and the detector system. In special applications windowless systems are sometimes used; the detection of boron K′X rays at 185 eV has been reported [13] in a system of this type. Problems associated with operating windowless systems make their use difficult for general purposes. Although the intrinsic efficiency of semiconductor detectors makes them sensitive to characteristic (either K or L) X rays of all elements from boron to uranium in the period table, the characteristics of the excitation and the energy resolution normally restricts the use of a spectrometer to a much smaller range of elements.

The energy resolution of a semiconductor detector spectrometer is determined partly by electronic noise but also by statistical fluctuation in the number of electron-hole pairs generated by monochromatic radiation. The RMS deviation of a monoenergetic X-ray line caused by these two sources of fluctuation can be expressed as the quadratic sum of two components

$$\sigma_{RMS} = \sqrt{\sigma_e^2 + \sigma_s^2} \qquad (3)$$

where σ_e is the electronic noise contribution and σ_s represents the statistical spread in the number of free charges produced in the detector. The electronic noise contribution is determined by the input amplifier stage and

by detector leakage current. Operating the detector at low temperatures is essential to reduce the latter component. The statistical spread σ_s can be represented by:

$$\sigma_s = \sqrt{F\ E\ \varepsilon} \tag{4}$$

where E is the X-ray energy, ε is the average energy required to produce an electron-hole pair and F is the Fano factor which corrects for the departure of the energy loss process from a Poisson distribution. Typical values are ε = 3.7 eV and F = 0.12 for Si, and ε = 3.0 and F = 0.10 for Ge. Comparison of these with the value of ε = 30 eV for gas detectors illustrates the inherent resolution advantage of semiconductor detectors. The lower value of both F and ε for Ge relative to Si accounts for slightly better resolution at high energies for Ge relative to Si. Figure 1(b) is a plot of Eq. (2) with appropriate values for ε and F for Si, allowing also for the contribution of electronic noise.

B. Signal Processing Electronics

In order to achieve the minimum possible resolution contribution due to electric noise sources it is necessary to filter the output signals to enhance the signal relative to noise. Figure 12 is a schematic of a typical signal channel employed with a semiconductor detector. The input preamplifier stage is mounted at the detector at low temperature in the cryostat. It integrates each detector charge signal to produce a voltage step proportional to the charge. This pulse is then amplified and shaped in a series of integrating and differentiating stages to achieve the optimum shape to maximize the signal/noise ratio. The resulting shaped pulse is then processed and stored in a multichannel pulse-height analyzer which accumulates the X-ray spectrum.

Figure 13 is an example of a spectrum obtained from a typical Si detector spectrometer showing the K X-rays of Mn together with a peak generated by a pulser. The resolution of the pulser peak is a measure of the electronic noise σ_e. The difference between the 99 eV pulser and the 165 eV Mn K_α widths

is due to the statistics of charge collection as expressed in Eq. (3) and (4). Electronic resolutions as low as about 60 eV have been achieved in special systems.

As compared with gamma-ray spectrometers, X-ray spectrometers are characterized by the large values of signal shaping times used to optimize energy resolution. Since these long pulse-shaping times place a severe limit on the maximum allowable counting rate, a shorter shaping time than the optimum (from the point of view of resolution) is used. Figure 14 is a plot of the counting-rate characteristics of a typical semiconductor system operated at various pulse-shaping times. The characteristic shaping time referred to in Fig. 14 is the time required for a Gaussian-shaped pulse to reach its maximum value and must be distinguished from the characteristic shaping time constant which can be considerably shorter. For the cases shown in Fig. 14, the best resolution is achieved at 17 μs peaking time. However, the output rate at high input counting rates is higher for the lower values of peaking times. Consequently a compromise value is often employed depending on the application.

The shape of the input/output data curves of Fig. 14 illustrate the effects of loss of pulses due to pulse pile-up. Since the signals arrive at random times, the time interval between pulses obeys a Poisson distribution. Following one event, the probability that a second event will occur within a time t is given by

$$P(t) = 1 - \exp(\lambda t) \tag{5}$$

where λ is the average rate in counts/second. At counting rates of 10^4 counts/sec there is a 40% probability of two events occurring within 50 μs of each other. Such pulses overlap and produce erraneous pulse amplitudes. To eliminate such ambiguous events, most spectrometer systems employ circuitry which detects such pulse pile-up and eliminates any signals contaminated in this way. The drop in output rate for high input rates as shown in Fig. 14 reflects the effect of pulse pile-up rejection. If lower counting rates are normally encountered, such as may be the case in radioisotope excitation, pile-up rejection may not be necessary.

Since pile-up rejection eliminates some of the valid events, an absolute measurement of the intensity of X-ray lines requires a method of correcting for these losses in the final data. Fortunately, the loss fraction is the same for all amplitudes in the spectrum so compensation can be affected by extending the total counting interval by the appropriate factor. The normal method is to use a live time clock system in which the counting time is determined by counting a predetermined number of periodic clock pulses which pass through the same rejection gate as the signals. If this system is properly designed the clock pulses undergo the same probability of rejection as the X-ray events.

Another method of overcoming pulse pile-up and dead time losses is possible if a pulsed X-ray tube is available. By shutting off the X-ray tube excitation immediately an event is detected and the probability of additional events occurring during the pulse processing time is reduced essentially to zero. At the end of the pulse processing time the tube is then turned on again and the next event is awaited. In such a system the output rate equals the input rate, no pile-up rejection is required and higher counting rates can be achieved.

Following the analogue signal processing just discussed, signals pass into an analogue-to-digital converter and thence are stored in a multichannel analyzer or small computer. The result is a spectrum of the number of detected events as a function of X-ray energy. This is the information which must be used to derive elemental concentrations.

Figure 15 is an example of a pulse amplitude spectrum obtained using Mo K X-ray excitation of an National Bureau of Standards orchard leaf sample. Elemental concentrations are indicated on the plot. The peak-to-background ratio for the fluorescent peaks is representative of current techniques.

IV. CALIBRATION METHODS

In this section we will analyze factors which determine the relationship between the concentrations of elements in the sample and the counting rate for the characteristic X rays in the detector. Only the simplest case will

be analyzed but the generalizations required to extend the analysis to other classes of samples will be indicated.

For the purpose of illustration we choose a sample in the form of a homogeneous slab of thickness d (cm) which is irradiated by photons of energy E_o and intensity I_o as illustrated in Fig. 16. To avoid cumbersome trigonometric functions, we will assume that the incident and fluorescent X rays have directions normal to the surface. To extend the analysis to other angles the appropriate distances can be divided by the cosines of the angle of incidence.

From the absorption expression of Eq. (1) we can write the intensity of fluorescence K or L radiation detected by the detector from the atoms of element i contained in a layer of thickness dx located at distance x below the surface of the sample as follows:

$$dI_i = \left[I_o e^{-\mu_o \rho x}\right]\left[\tau_i \rho_i \omega_i \varepsilon_i dx\right]\left[e^{-\mu_i \rho x}\right] \qquad (6)$$

The brackets logically separate the three components as follows:

i) The intensity of the incident flux transmitted by a thickness x, density ρ and average total mass attenuation μ_o for the incident ratiation.

ii) The fraction of the X rays reaching the element of thickness dx which interact in the element to produce vacancies in the K or L shells of element i followed by X-ray emission. The number of vacancies is $\tau_i\ \rho_i\ dx$. The fluorescence yield is ω_i. For convenience ε_i, the detector efficiency which is a function of the energy E_i, is also included in this term.

iii) The probability that the fluorescence X rays of energy E_i will escape back to the surface of the sample from a depth x in a medium with average mass absorption coefficient μ_i.

Integration of Eq. (6) over the sample thickness d gives the following expression for the total intensity of fluorescence radiation observed by the detector:

$$I_i = I_o\, G\, \tau_i \rho_i \omega_i \varepsilon_i \, \frac{1 - e^{-(\mu_i+\mu_o)\rho d}}{(\mu_i+\mu_o)\rho} \tag{7}$$

where the factor G is an efficiency term determined by the effective solid angle from the sample to the detector.

Two limiting cases of practical importance can be calculated. For very thin samples in which absorption and interelement effects are negligible $[\mu_i+\mu_o]\rho d << 1$, and the expression reduces to:

$$I_i = \left\{ I_o\, G\, \tau_i \omega_i \varepsilon_i \right\} \rho_i d \tag{8}$$

where the quantity $\rho_i d$ is the concentration of the element of interest in gm/cm^2

The quantity in brackets relates the concentration of the sample to the observed counting rate in the simplest of cases. Calculation of this 'relative X-ray excitation probability' can be performed using published values for τ_i and ω_i [14-16]. The results of these calculations were shown in Fig. 8. The fact that these curves are smoothly varying functions of atomic number has important consequences for quantitative multielement analysis. If the system has been carefully calibrated for a given element then an approximate result for a neighboring element can be easily inferred from a crude plot of Eq. (8). R. Giauque, et al have refined the technique using a semiempirical approach to the evaluation of this function and have obtained accurate calibrations extending over a wide range of atomic numbers. Table 2 is a comparison of measured and calculated results for thin film standards. These authors have also extended the method to include an attenuation correction of Eq. (6) for moderately thin homogeneous samples in which the exciting radiation is not severely attenuated. This calibration technique will permit analysis of a wide class of samples such as air pollution filters and many biological specimens.

The second special case of Eq. (7) involves very thick samples in which $\rho d \to \infty$. In this case the expression reduces to

$$I_i = \frac{I_o G \tau_i \omega_i \varepsilon_i}{[\mu_i + \mu_o]} \frac{\rho_i}{\rho} \tag{9}$$

This equation can be applied to samples in which the absorption of the matrix is known beforehand (i.e., μ_i and μ_o) and the concentration ρ_i is not large enough to significantly alter the matrix absorption. This is normally so in trace element analysis.

The extension of these ideas from monoenergetic excitation to broad-energy excitation involves a second sum or integration of Eq. (7) over the incident energy distribution. This can be done using parametric expressions for μ and τ together with measured X-ray distributions. Alternatively a totally empirical approach can be used. The qualitative features of a calibration curve generated experimentally are similar to those discussed for monoenergetic excitation.

In order to use these semiempirical formulae for accurate analytical purposes, it is necessary to prepare samples in the right form. Ideal samples are homogeneous and must be dilute to avoid interelement X-ray enhancement effects. Techniques for preparing such samples are discussed elsewhere in this book. In situations where these requirements are not met and where interelement and absorption effects may be important, a more elaborate calibration procedure must be undertaken. In its most general formulation, the intensity of X rays produced by element i depends on the concentration of all other elements in the sample. This can be expressed as follows

$$\rho_i = I_i / \sum_j a_{ij} I_j \tag{10}$$

The quantitative a_{ij} represent a relative measure of the absorption of enhancement effect of element j on the observed intensity I_i. The problem of calibration then involves the determination of the coefficients a_{ij}. A number of methods of doing this have been developed [17,18]. This problem is also present in the case of wavelength-dispersion analysis but that the

spectrum obtained from an energy-dispersive spectrometer can give a simultaneous measurement of I_i for all elements of interest. These and related topics are discussed in the chapter on data interpretation. These complications are avoided by preparing standards which closely approximate the form of the unknown sample; this method becomes even more desirable as the sample form departs far from the simple case discussed earlier. Where interelement and matrix effects are important, and the number of constituent elements is not large, the solution of Eq. (7) can be effectively accomplished by using calibration curves. As the sample departs far from uniformity and homogeneity, it becomes essential that a standard sample closely replicating the main constituents of the unknown be prepared.

The question of sample homogeneity closely relates to the particle size problem often encountered in X-ray fluorescence analysis. With the increasing importance of energy-dispersive analysis applied to air particulate analysis an understanding of this effect is desireable. Figure 16(b) illustrates the problem of measuring the X-ray intensities from an irregularily shaped particle. Defining a characteristic absorption length $(\mu\rho)^{-1}$ then, if the average diameter of the particle is comparable to or greater than this length there will be a large difference between the output intensities I_i and I_i' arising from different parts of a particle. In this case the measured intensity may be a function of the distribution of particle sizes in powder specimens, or of surface irrgularities in solid samples. Rhodes has treated the question of a generalized particle size distribution and derives models for various distributions [19]. T. Dzubay has derived correction factors to be used for air particulate analysis assuming that the particles are spherical [20]. Criss has calculated the particle size correction for a variety of shapes and compositions [21]. In any of these approaches, assumptions must be made regarding the particle composition and shape before a reasonable correction can be applied. To overcome this, R. Giauque, et al have used a variable excitation energy to measure the fluorescence output as a function of the penetration depth of incident X ray beam. Since these corrections are only approximate, the particle size effects always limit accuracy, particularly when analyzing for low Z elements.

V. SPECTRAL ANALYSIS

The earlier discussion of calibration techniques assumes that an accurate measure of X-ray line intensities could be derived from the multichannel fluorescence spectrum. This is clearly easy for high concentration elements where a simple summation over the channels in the peak is adequate. However, in the general case, the size of the peak of interest must be derived despite the presence of continuous background and interference from lines due to other elements in the sample. The accurate subtraction of continuous background is particularly important in trace analysis applications where the peaks are small. In large scale analysis programs, this must be done accurately and rapidly.

Figure 17 helps illustrate the complexity of the problem of spectral analysis. This example is from a typical air pollution sample consisted of the collected particulates on a 5 mgm/cm^2 cellulose backing. The sample was irradiated with Mo K X rays. The logarithmic plot emphasis the number of details which must be included in a successful analysis procedure. For example the continuous background beneath the peaks in the region between Ca and Br is very difficult to define since the density of peaks obscures any reference level which might exist. The number of elements present requires careful consideration of the possible overlap of lines from adjacent elements and of their K X rays with the complex L X-ray spectrum of Pb. Often, the spectra to be analyzed are much simpler than this but a general purpose computer program should be capable of handling all types of problems.

The simplest method for extracting peak areas is to sum the data over a selected channel interval, typically the K_α or L_α X ray, after subtraction of a continuous background. Interferences between elements can be handled by a sequential substraction of the overlaping lines using the known ratios between K_α and K_β to determine the amount of overlap. In cases where the number of interelement interferences are few and the background can be easily determined, this simple method can be used effectively.

The next level of sophistication involves the use of fitting routines in which the background and peaks are compared to reference standards on a point for point basis. The comparison can be performed either by a simple sum over the peaks of interest or by least squares techniques.

The background is usually estimated either by interpolation over a limited region or by relating the background at a given point to the intensity of scattered radiation at the high energy region of the spectrum. The standard peak shapes can be generated mathematically using Gaussian peak shapes of appropriate width and locations and intensities specified by previously known data. Difficulties with the mathematical method of peak generation arise where the characteristic X-ray lines become complex such as the L X rays of heavy elements or the partially resolved $K_{\alpha_1} - K_{\alpha_2}$ doubled for $Z > 40$.

An alternative method for generating peak shapes is to experimentally measure the spectrometer response to X rays of a given element and store that spectrum in the computer [23]. This has the advantage that multiple structure and non Gaussian peak shapes are automatically determined. The cost of the added storage capacity required is offset by the simplifications involved in programming. The advantages of using standard shapes and more complicated fitting routines are a slight increase in the statistical accuracy of the measurement and a more flexible approach to the problem of interelement interferences. However, the program can be extremely complex particularly if a large number of elements are to be simultaneously analyzed and do not fit easily into a small computer.

The next level of mathematical complexity involves the use of transformation techniques to enhance the peak to background ratio prior to spectrum unfolding. Three examples of interest are Fourier analysis [24], digital filtering [25], and correlation techniques [26]. Although each is slightly different they are all basically methods whereby the mathematical transformation filters out the smoothly varying background subtraction and can be incorporated into small computer systems. On the other hand, the problems of multiple lines and interelement interference must be handled separately.

As yet no completely general method of X-ray spectral analysis has been developed. Various combinations of the above techniques are used by a number of laboratories and commercial manufacturers with varying success depending on the type of application. It is probable that all the available programs achieve the same level of accuracy for the more straightforward problems and fail equally in the more complicated situations. The reasons for this

lie not only in the complexity of multiple element spectra but also in instrumental effects which are difficult to compensate mathematically. These effects include small gain shifts in the spectrometer as a function of time, changes in peak shape and location as the count rate varies, and variations in the relative intensities of the characteristic X ray for a particular element due to absorption effects. Since these problems are not easily corrected in typical programs, the subsequent spectral analysis is subject to large errors particularily in the case of the less intense peaks. The net effect is to limit the dynamic range over which elemental concentration can be determined.

VI. APPLICATIONS

Areas in which energy dispersive analysis has been successfully employed are numerous and have been reported extensively in the literature. In most respects the applications duplicate those of conventional X-ray fluorescence. Applications range from on-line process control where only one or two elements must be continuously monitored to environmental analysis applications where a complete list of elements and their absolute concentrations must be determined. Some specific areas of interest are also discussed elsewhere in this volume.

VII. CONCLUSION

The technique of energy-dispersive photon-excited X-ray fluorescence analysis has been developed to the point where it constitutes a potent analytical tool for accurate and sensitive nondestructive multiple-element analysis. A number of instruments based on this method are now commercially available. As they become more widely used the full range of applications of the technique will no doubt be expanded.

REFERENCES

1. J. V. Gilfrich, P. G. Burkhalter and L. S. Birks, Anal. Chem., 45: 2002 (1973).
2. E. H. S. Burhop and W. N. Asaad, Adv. At. Mol. Phys., 8: 163 (1972).
3. J. W. Cooper, Nucl. Instr. and Methods, 106: 525 (1973).
4. W. H. McMaster, N. Kerr Del Grande, J. H. Mallet and J. H. Hubbell, Lawrence Livermore Laboratory Report UCRL-50174 (1970).
5. J. R. Rhodes, "Design and Application of X-ray Emission Analyzers Using Radioisotope X-ray or Gamma Ray Sources" in Energy Dispersion X-ray Analysis: X-ray and Electron Probe Analysis, ASTM Special Technical Publication 485: 243 (1970).
6. R. D. Giauque, F. S. Goulding, J. M. Jkalevic and R. H. Pehl, Anal. Chem., 45: 671 (1973).
7. J. C. Russ, A. O. Sandborg, M. W. Barnhart, C. E. Soderquist, R. W. Lichtinger and C. J. Walsh, Adv. X-ray Anal., 16: 284 (1973).
8. T. G. Dzubay, B. V. Jarrett and J. M. Jaklevic, Nucl. Instr. and Methods, 115: 297 (1974).
9. L. Kaufman and D. C. Camp, Adv. X-ray Anal., 18: 2 (1975).
10. R. H. Howell, W. L. Pickles and J. L. Cate, Jr., Adv. X-ray Anal., 18: 265 (1975).
11. F. S. Goulding, J. M. Jaklevic, B. V. Jarrett and D. A. Landis, Adv. X-ray Anal., 15: 470 (1972).
12. J. M. Jaklevic and F. S. Goulding, IEEE Trans. Nucl. Sci., NS-19, No. 3: 384 (1972).
13. J. S. Hansen, J. C. McGeorge, D. Nix, W. D. Schmitt-Ott, I. Unus and R. W. Fink, Nucl. Instr. and Methods, 106: 365 (1973).
14. W. J. Gallagber and S. J. Cipolla, Nucl. Instr. and Methods, 122: 405 (1974).
15. Bambynek, et al, Rev. Mod. Phys., 44: 716 (1972).
16. J. S. Hansen, H. V. Frevnd and R. W. Fink, Nucl. Phys., A142: 604 (1970).
17. L. S. Birks, in X-ray Spectrochemical Analysis, Vol. II, Chemical Analysis, John Wiley & Sons, New York 1969.

18. R. O. Muller, in Spectrochemical Analysis by X-ray Fluorescence, Plenum Press, New York (1972).

19. J. R. Rhodes and C. B. Hunter, X-ray Spectrometry, 1: 113 (1972).

20. T. G. Dzubay and R. O. Nelson, Adv. X-ray Anal., 18: 630 (1975).

21. J. W. Criss, Anal. Chem., 48: 179 (1976).

22. R. D. Giauque, R. B. Garrett, L. Y. Goda, J. M. Jaklevic and D. F. Malone, Adv. X-ray Anal., 19: 305 (1976).

23. J. M. Jaklevic, B. W. Loo and F. S. Goulding, "Photon Induced X-ray Fluorescence Analysis Using Energy Dispersive Detector and Dichotomous Sampler" to be published in X-Ray Fluorescence Analysis of Environmental Samples, 1976. Lawrence Berkeley Laboratory Report LBL-4834.

24. N. G. Volkov, Nucl. Instr. and Methods, 113: 483 (1973).

25. T. Inouye, T. Harper and N. C. Rasmussen, Nucl. Instr. and Methods, 67: 125 (1969).

26. A. Robertson, W. V. Prestwich and T. J. Kennett, Nucl. Instr. and Methods, 100: 317 (1972).

FIGURE CAPTIONS

FIG. 1. Energy resolution capabilities of X-ray detectors. a) Comparison of typical semiconductor detector with a proportional counter and a Bragg crystal spectrometer. b) Resolution expressed as the full width at half maximum for a typical semiconductor system as a function of energy.

FIG. 2. a) The energies of the principal X-ray absorption edges and emission lines as a function of atomic number.
b) Energy differences between adjacent X-ray lines of the elements. These curves should be compared with the resolution curve in Fig. 1(b).

FIG. 3. Schematic of the X-ray fluorescence process.

FIG. 4. Cross section for inner shell vacancies formation as a function of exciting photon energy.

FIG. 5. Energy and angle dependence of the Compton effect (inelastic scattering).

FIG. 6. Idealized X-ray fluorescence spectrum resulting from excitation of trace elements in a low atomic number matrix using monoenergetic photons.

FIG. 7. Schematics of typical radioisotope and X-ray tube fluorescence geometries in both direct and secondary fluorescence configurations.

FIG. 8. Probability of X-ray production as a function of energy of the characteristic X rays for three different exciting radiations.

FIG. 9. Cross section of a typical lithium drifted silicon semiconductor detector.

FIG. 10. Cross section of a top-hat detector geometry a) and a guard ring detector b) showing the internal field distributions.

FIG. 11. Calculated efficiencies of Ge and Si detectors as a function of incident X-ray energy.

FIG. 12. Schematic of complete X-ray spectrometer system.

FIG. 13. Spectrum of Mn K X rays together with a pulser peak.

FIG. 14. Output counting and energy resolution rate as a function of input counting rate for a pulsed optical-electronic processor employing pile-up rejection.

FIG. 15. Fluorescence spectrum obtained using Mo K X-ray excitation on a National Bureau of Standards Orchard leaf specimen.

FIG. 16. Diagrams showing the mechanism X-ray absorption corrections for a) a uniform layer and b) an irregular particle. In the latter case I_i and I_i' due to the difference in absorption paths.

FIG. 17. A typical fluorescence spectrum obtained with an air pollution sample. Note the density of peaks and the subsequent lack of regions from which a smooth background might be estimated.

TABLE 1

Radioisotopes For X-ray Fluorescence

Nuclide	Half-Life	Emission Energies
^{55}Fe	2.7 years	5.9 keV
^{109}Cd	453 years	22.1 keV, 87.7 keV
^{125}I	60 days	27 keV
^{241}Am	458 years	12-17 keV, 60 keV
^{57}Co	270 days	6.4 keV, 122 keV, 144 keV
^{238}Pu	86.4 years	12-17 keV

TABLE 2

Relative Excitation Efficiencies

Peak	Calculated Intensity	Standard Value
Cr K_α	.381	.370 ± .011
Mn K_α	.450	.435 .003
Fe K_α	.587	.559 .003
Ni K_α	.884	.882 .007
Cu K_α	1.000*	1.000 .015*
As K_α	1.653	1.660 .083
Se K_α	1.776	1.753 .057
Pb L_α	.804	.774 .019

* Values are normalized for Cu K_α

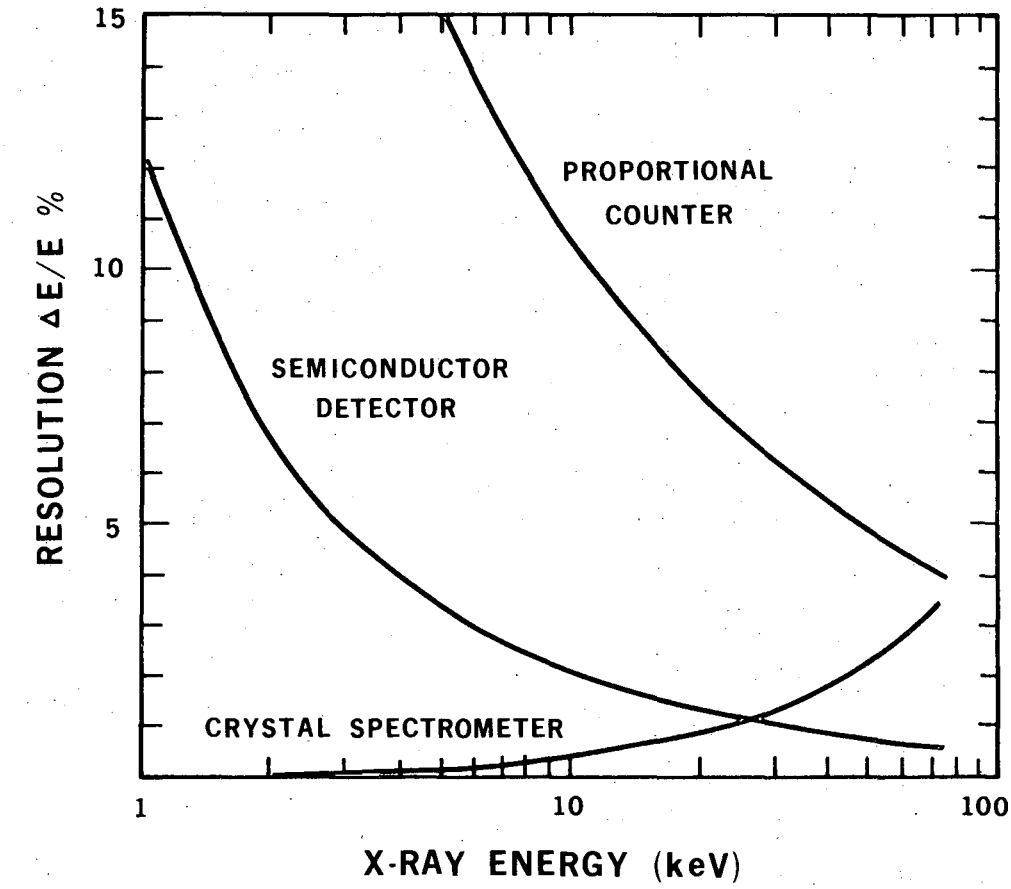

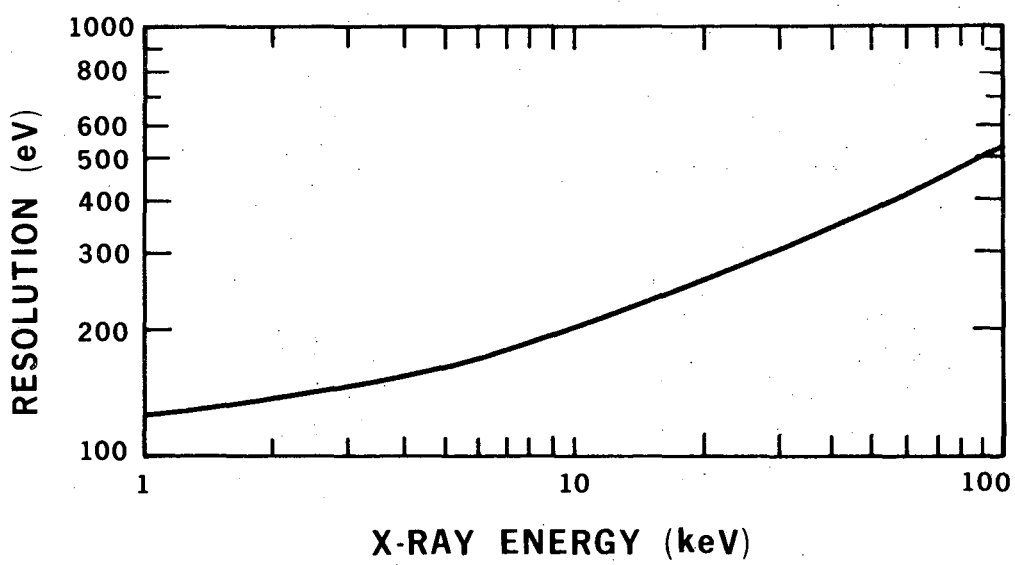

XBL 755-1328

Fig. 1 a) and b)

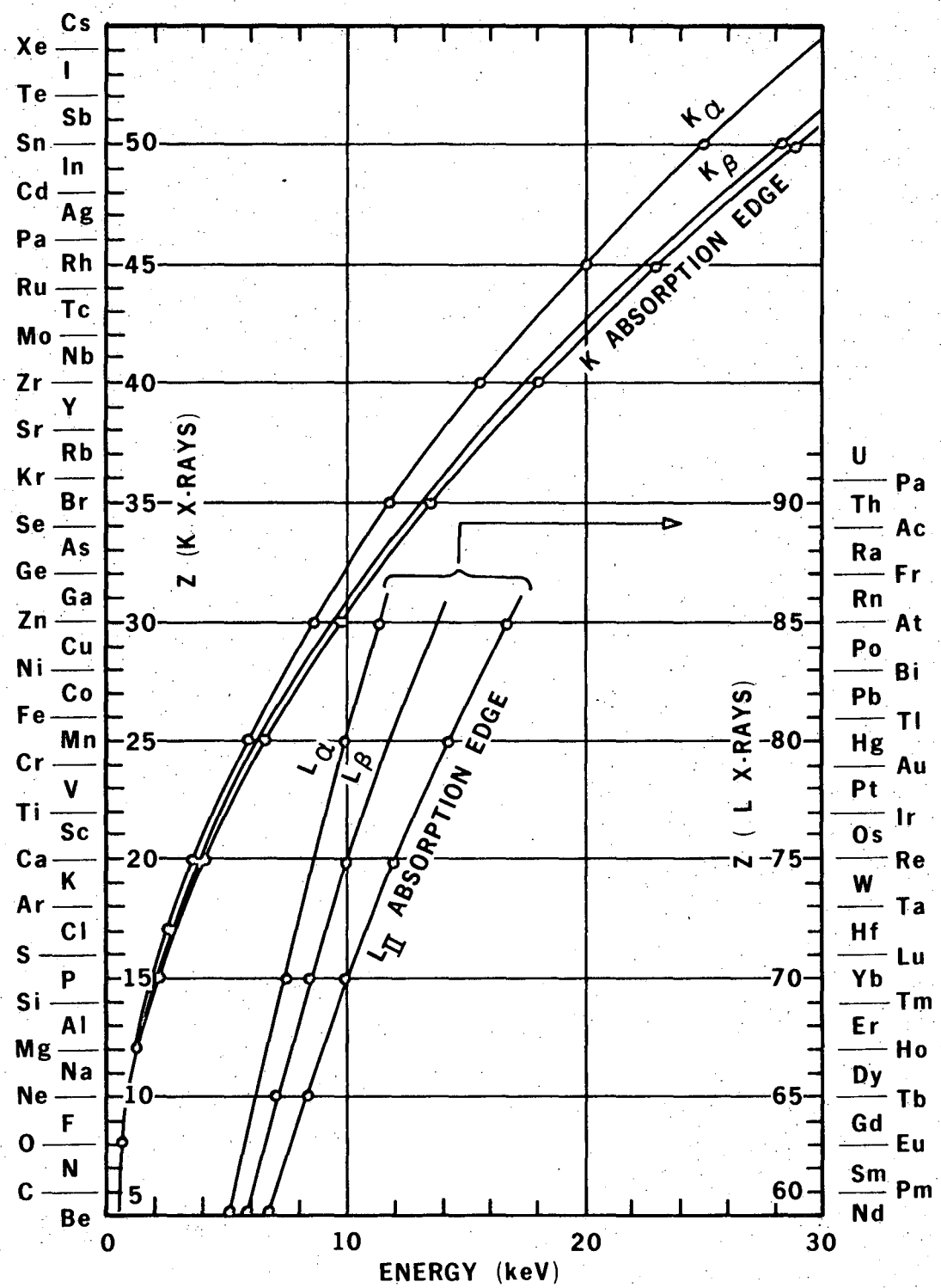

XBL 733-283

Fig. 2 a)

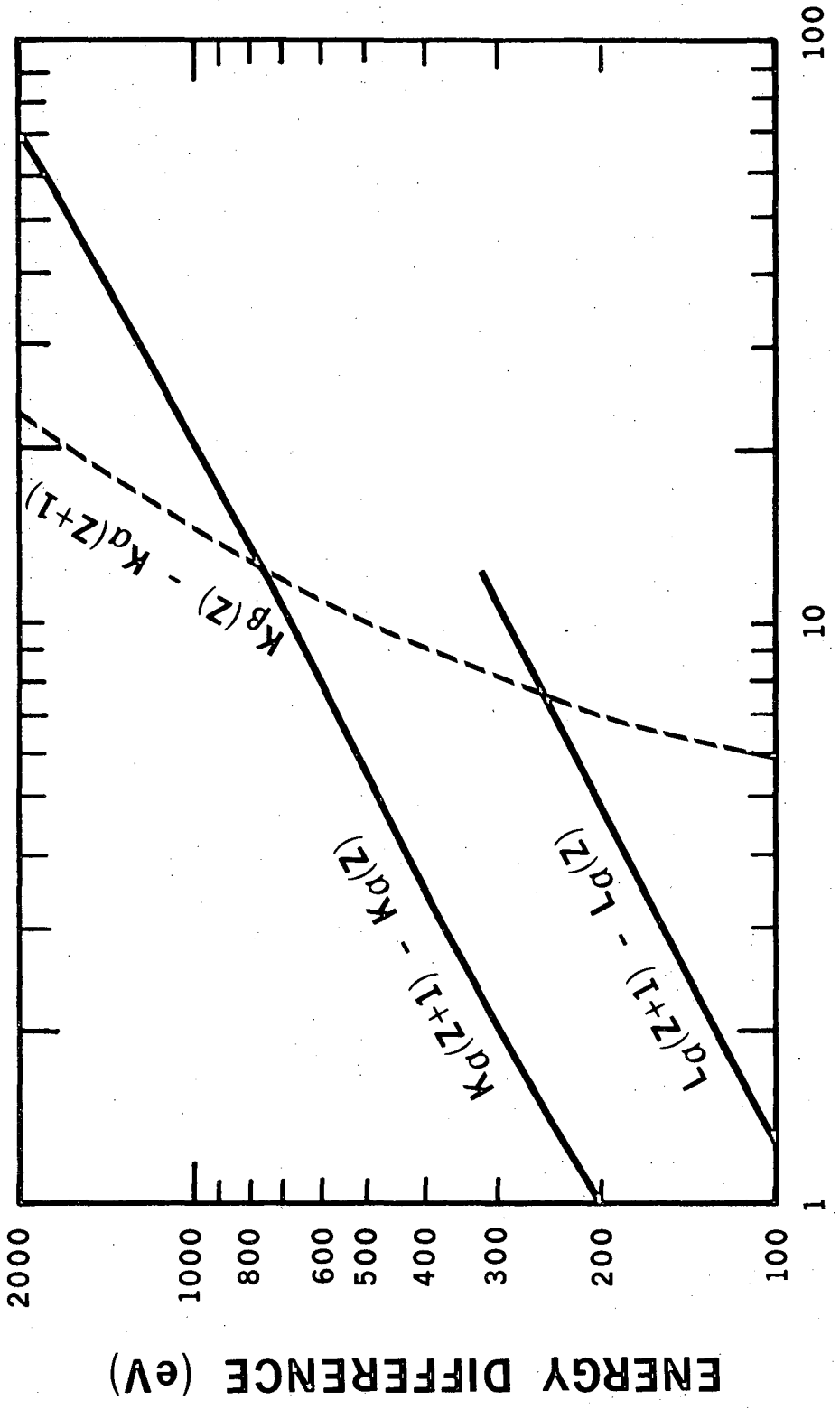

XBL 755-1388

Fig. 2 b)

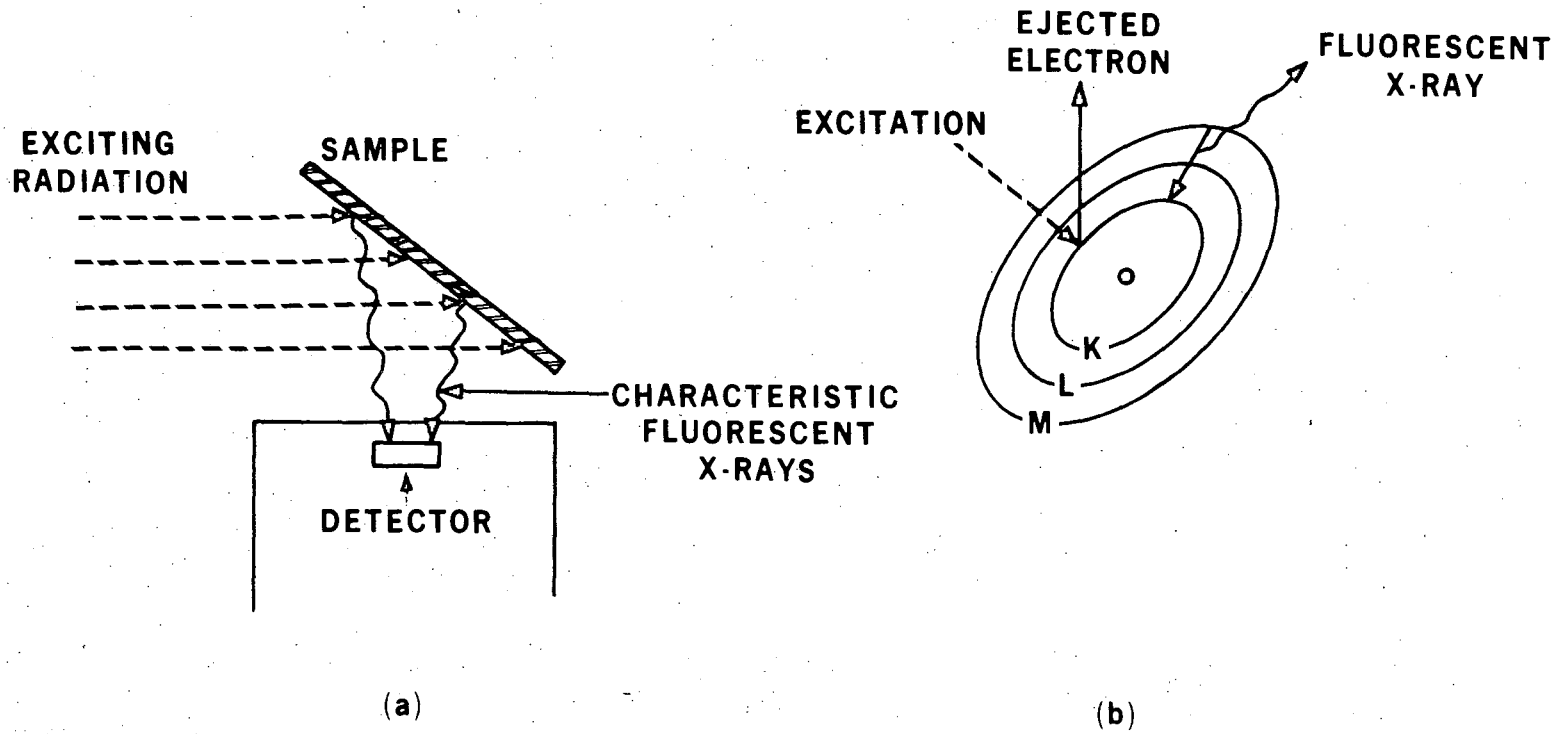
EXCITING
RADIATION
SAMPLE
CHARACTERISTIC
FLUORESCENT
X-RAYS
DETECTOR
(a)
EJECTED
ELECTRON
FLUORESCENT
X-RAY
EXCITATION
O
K
L
M
(b)

Fig. 3

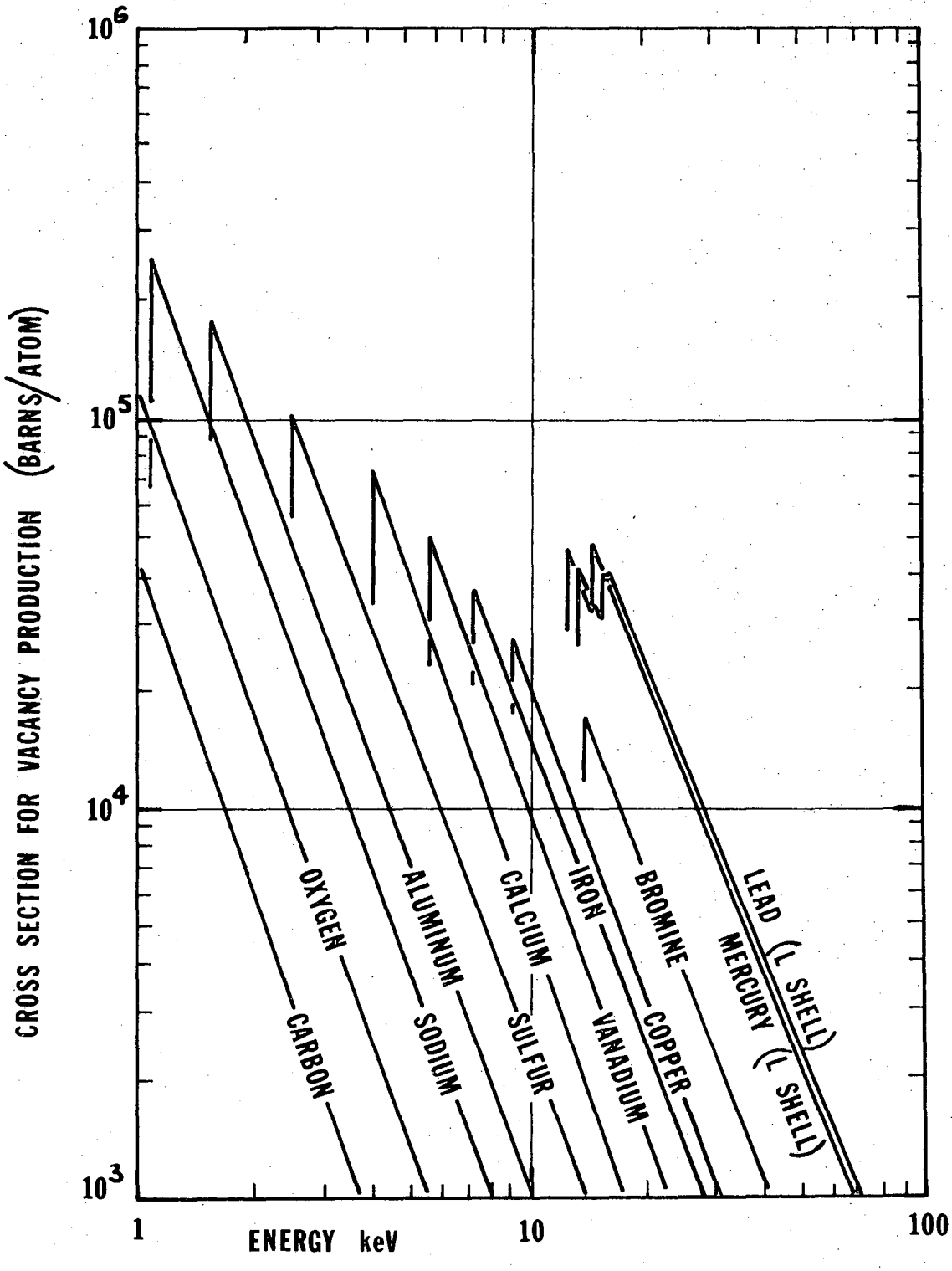

XBL 713-564

Fig. 4

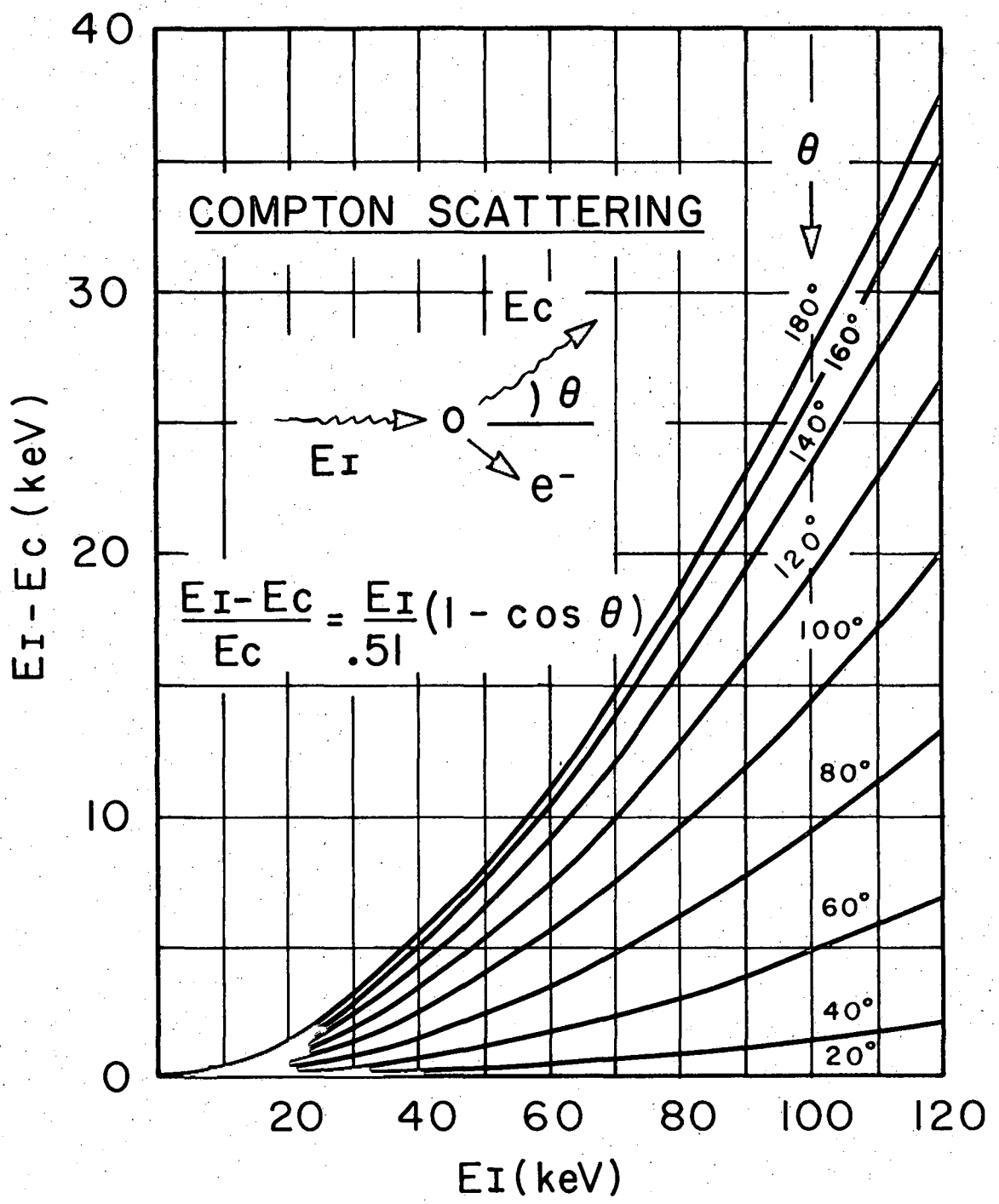

XBL 713-387

Fig. 5

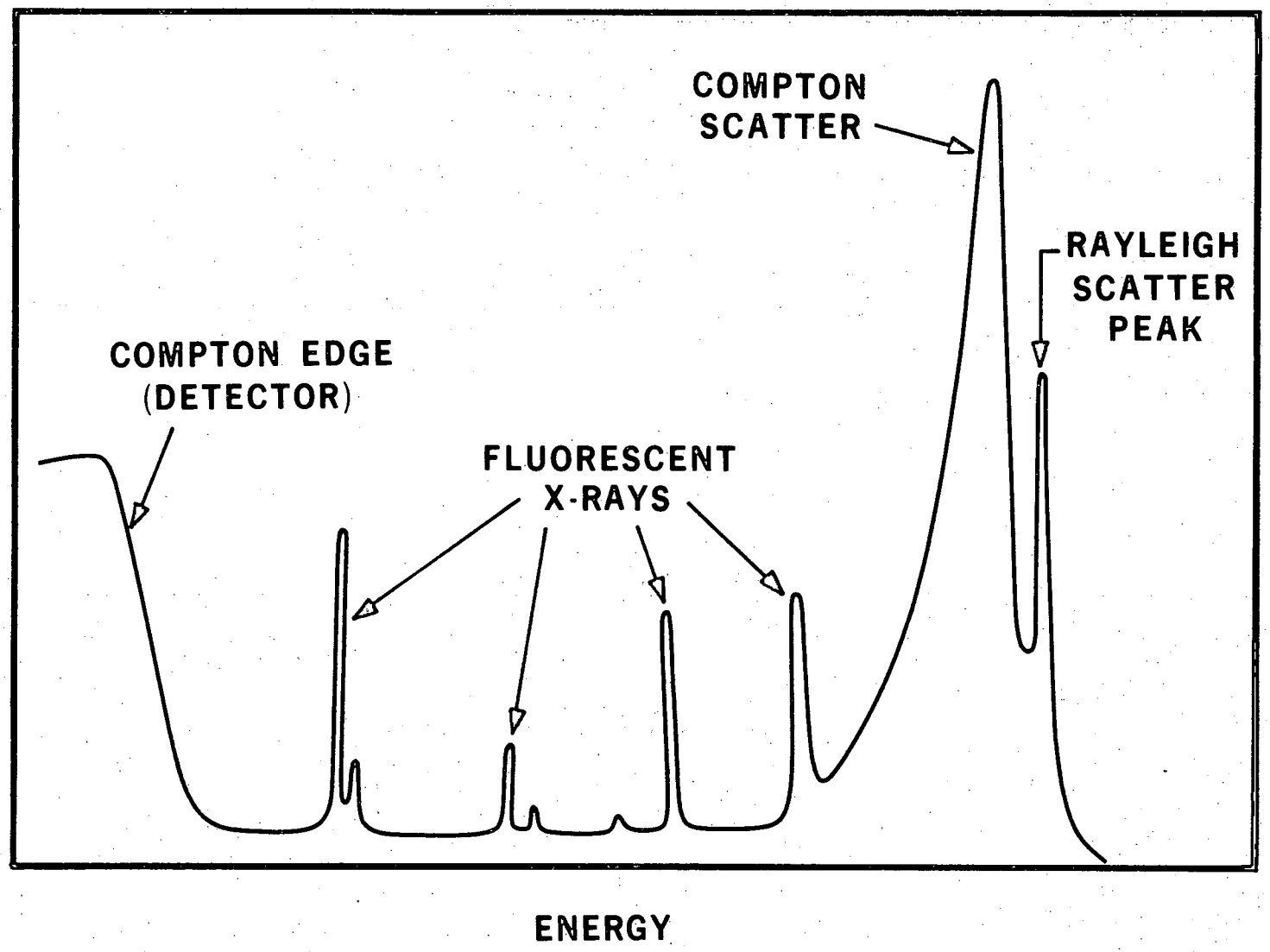

XBL 733-292

Fig. 6

RADIOISOTOPE EXCITATION

A) DIRECT

B) SECONDARY FLUORESCENCE

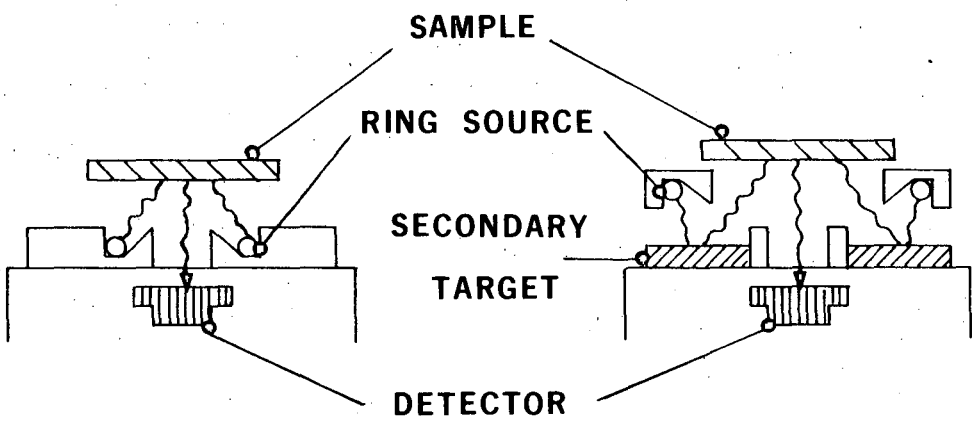

X-RAY TUBE EXCITATION

A) DIRECT

B) SECONDARY FLUORESCENCE

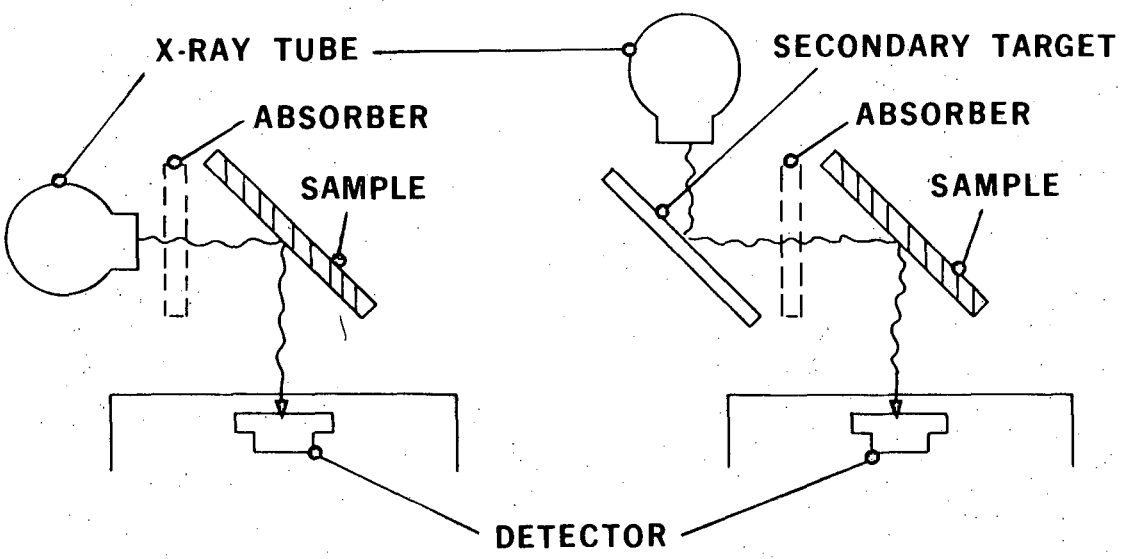

Fig. 7

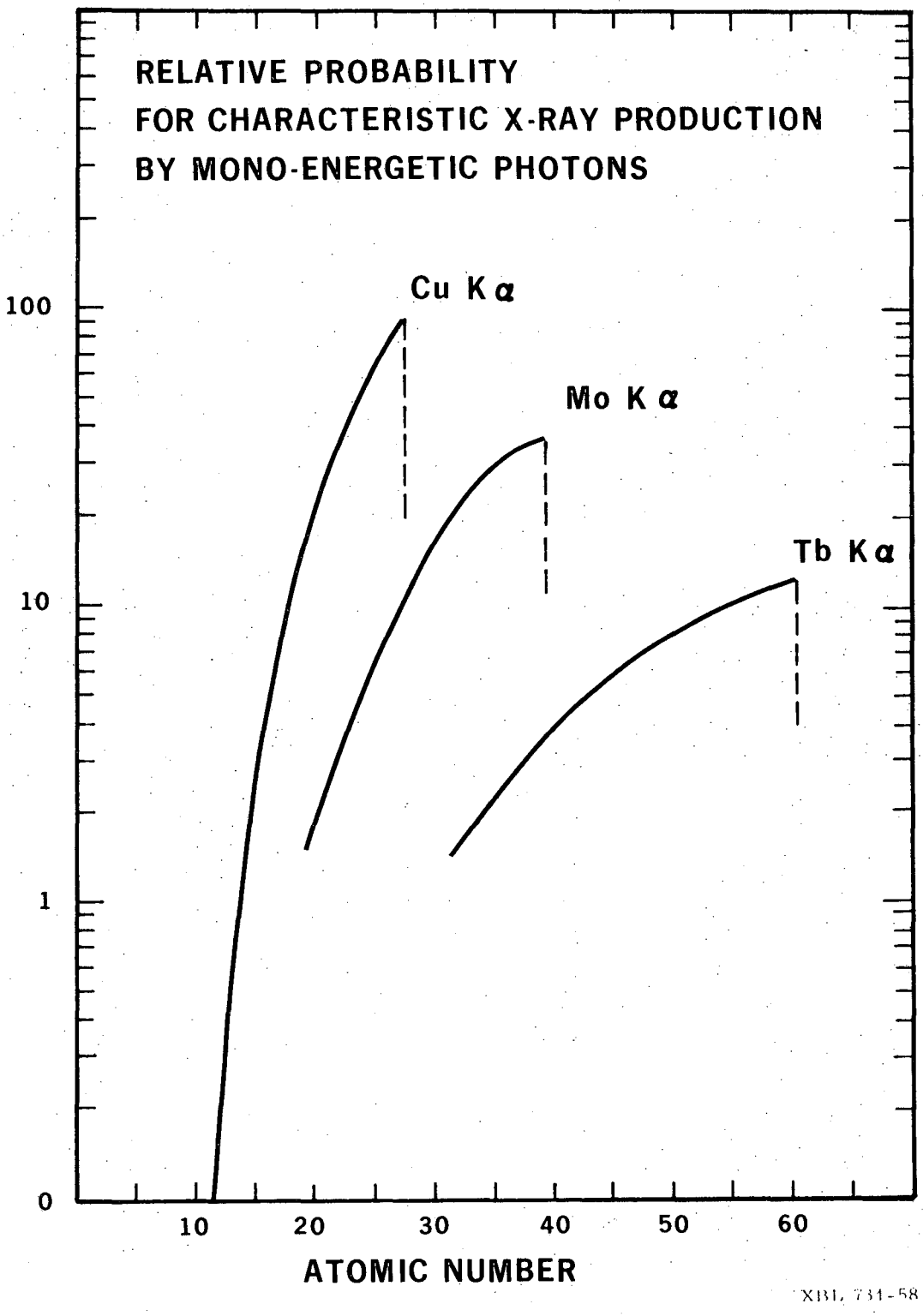

Fig. 8

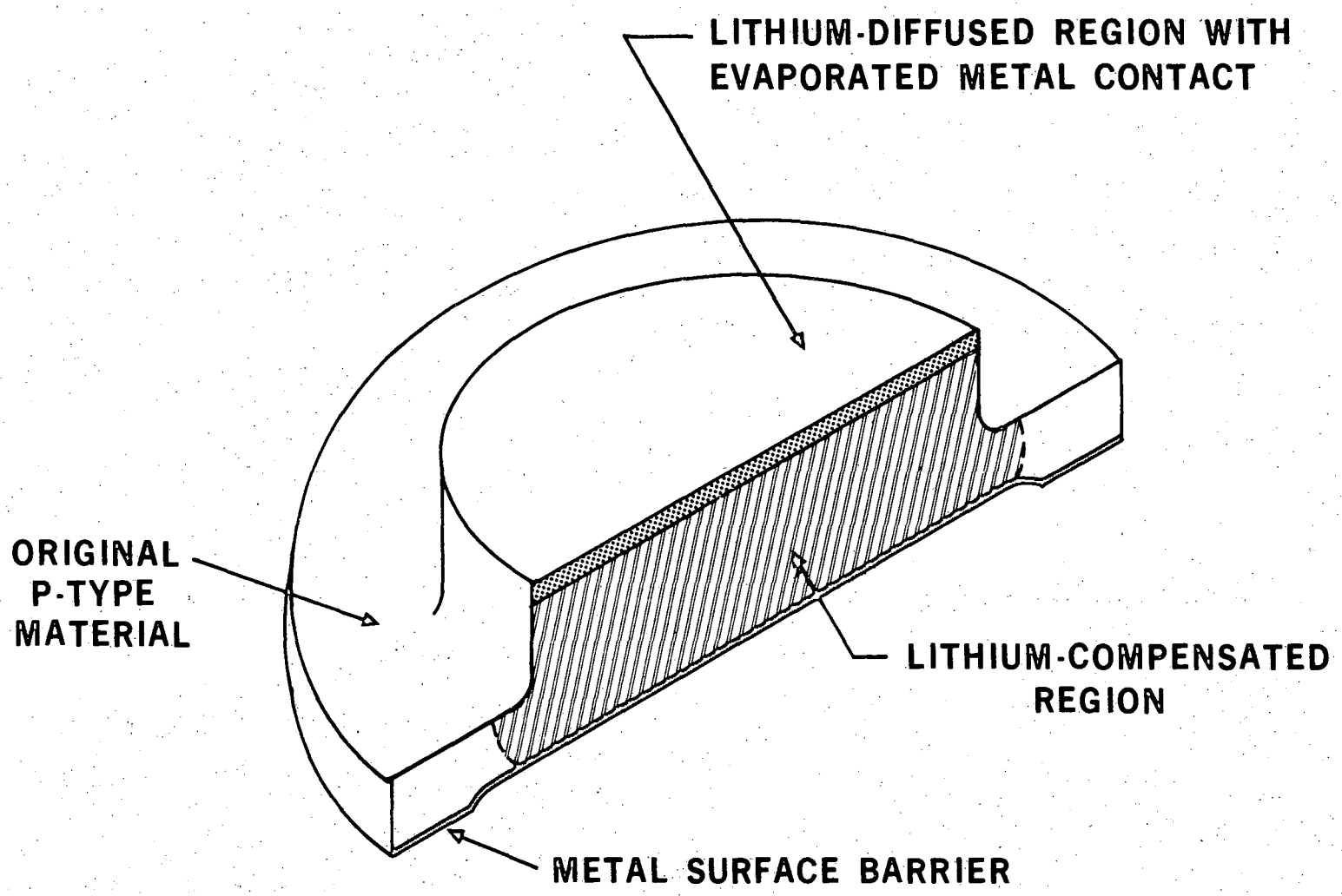

XBL 728-1492

Fig. 9

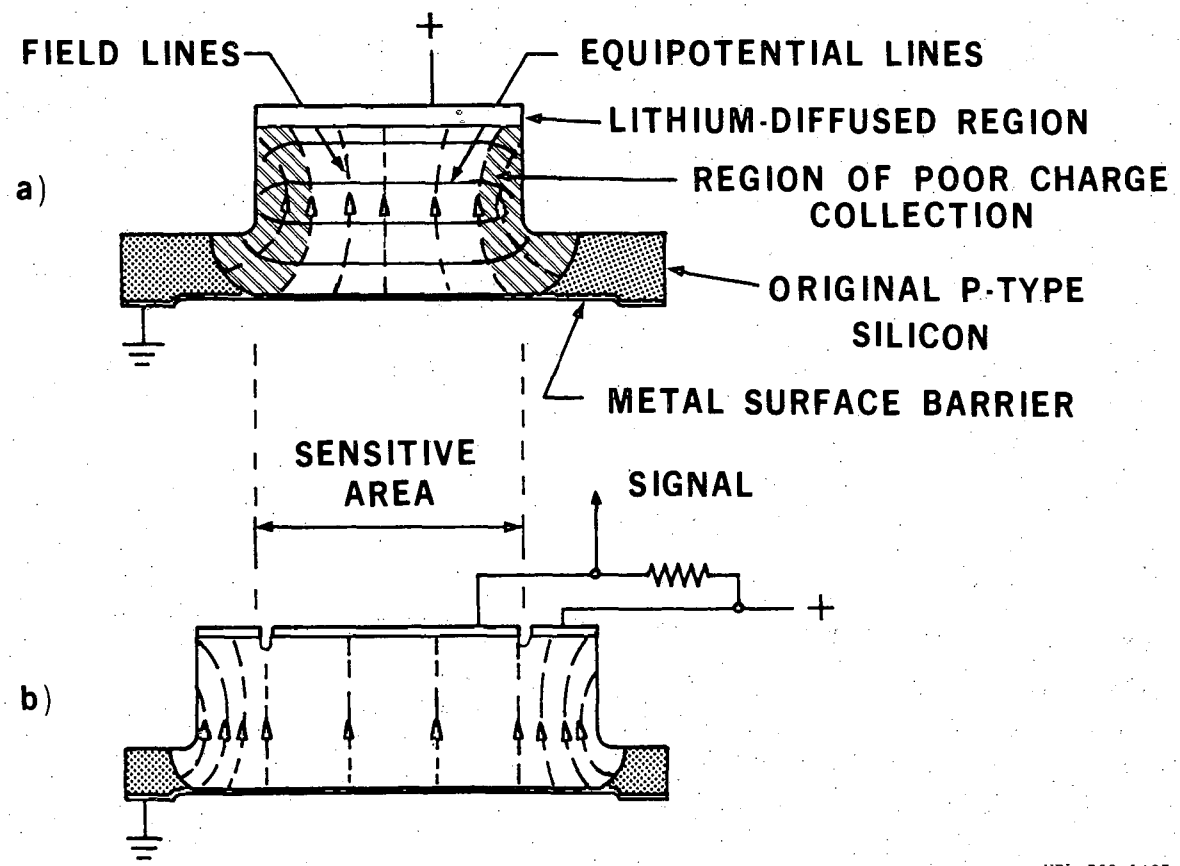

Fig. 10 a) and b)

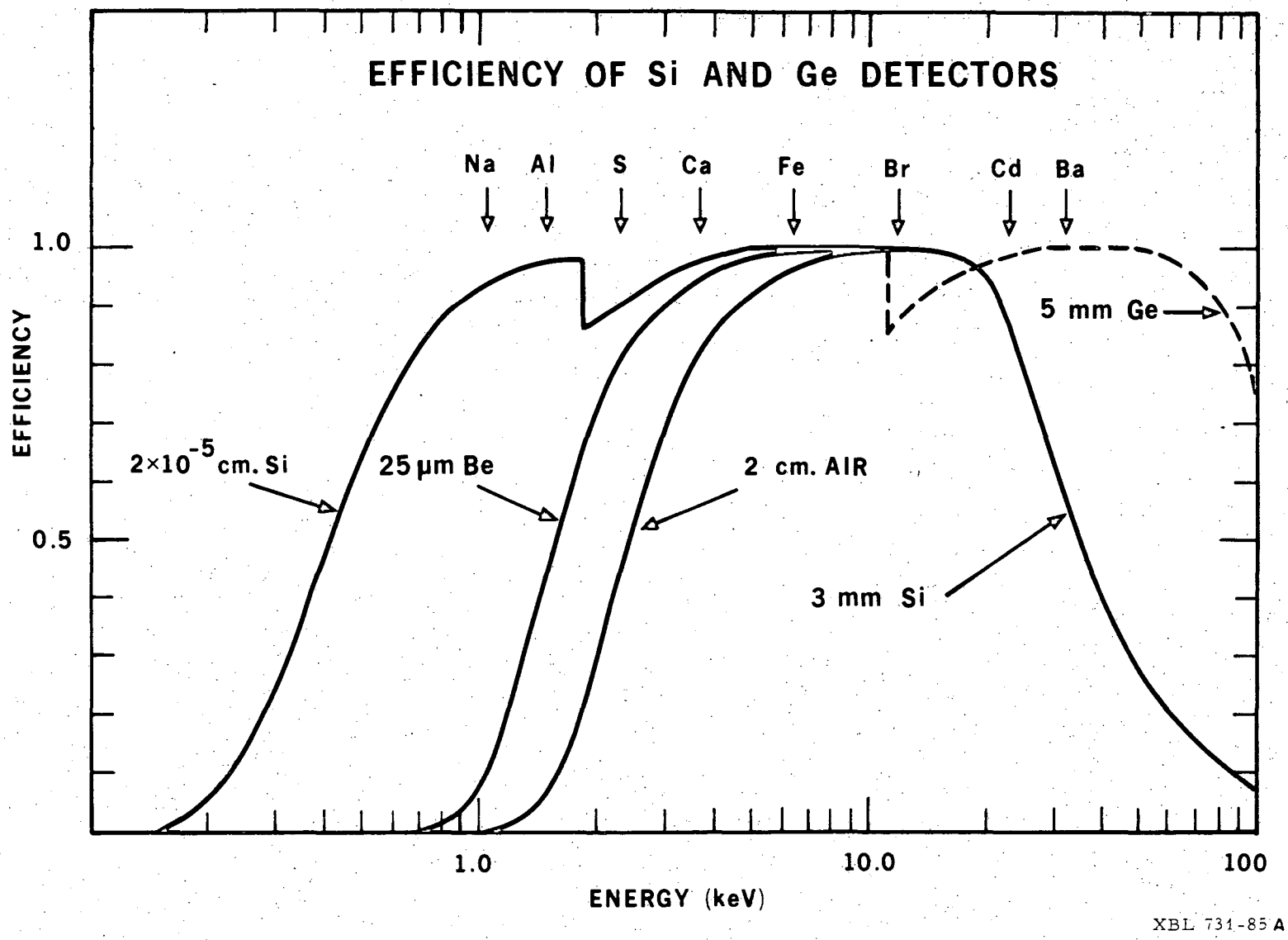
EFFICIENCY OF Si AND Ge DETECTORS
Na
Al
S
Ca
Fe
Br
Cd
Ba
1.0
0.5
EFFICIENCY
2×10-5 cm. Si
25 µm Be
2 cm. AIR
3 mm Si
5 mm Ge
1.0
10.0
100
ENERGY (keV)
XBL 731-85 A

Fig. 11

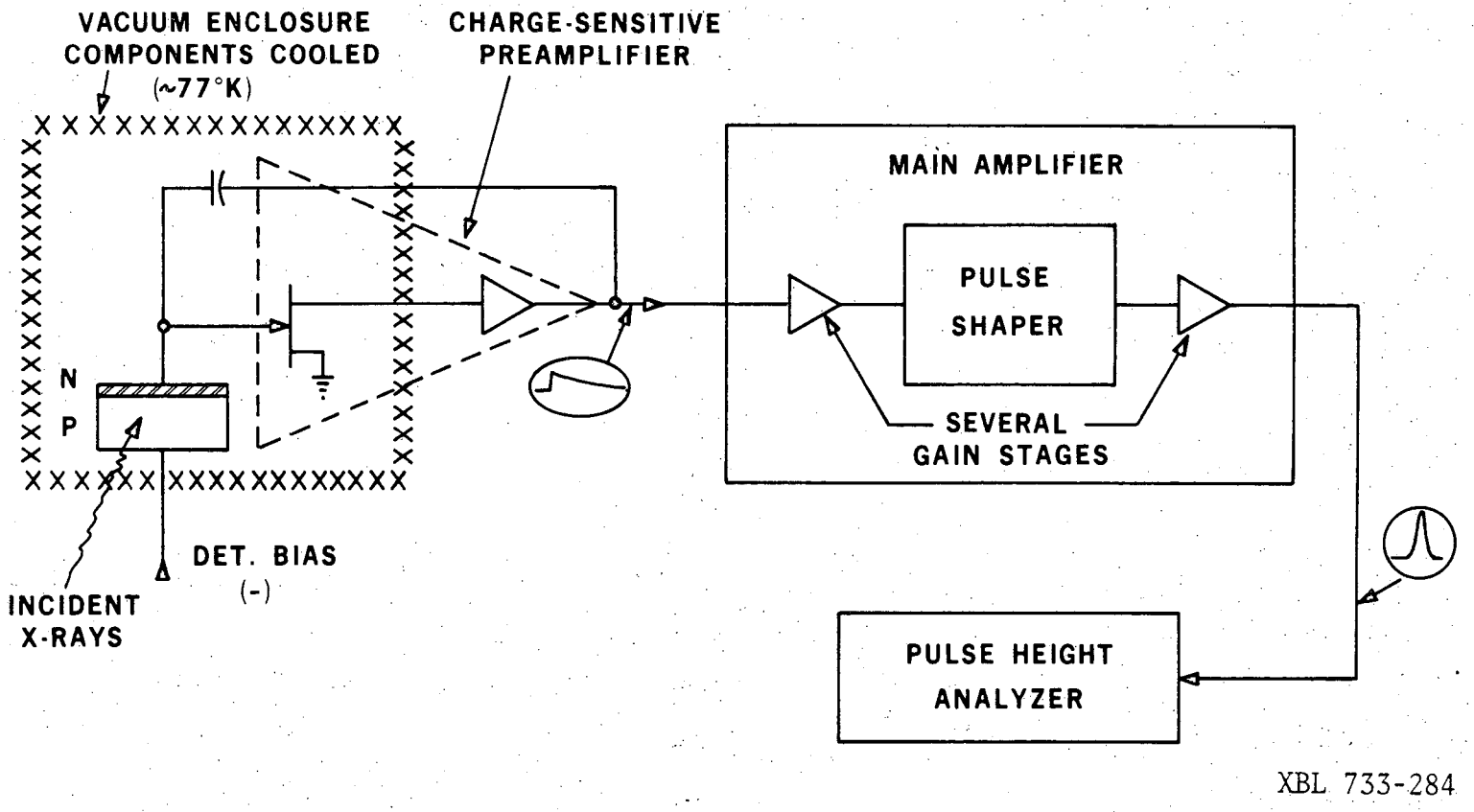

Fig. 12

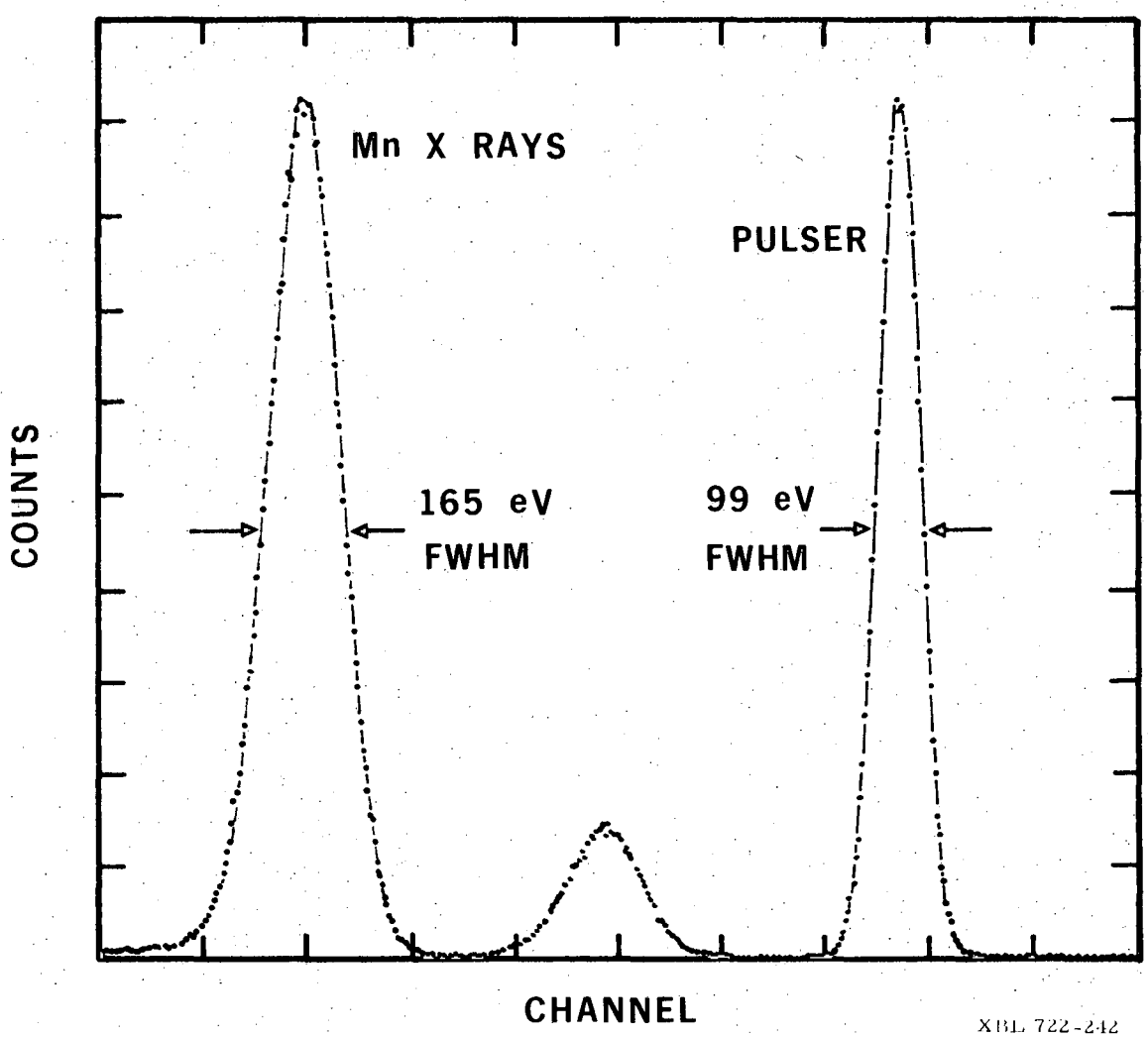
Mn X RAYS
PULSER
165 eV
FWHM
99 eV
FWHM
COUNTS
CHANNEL
XBL 722-242

Fig. 13

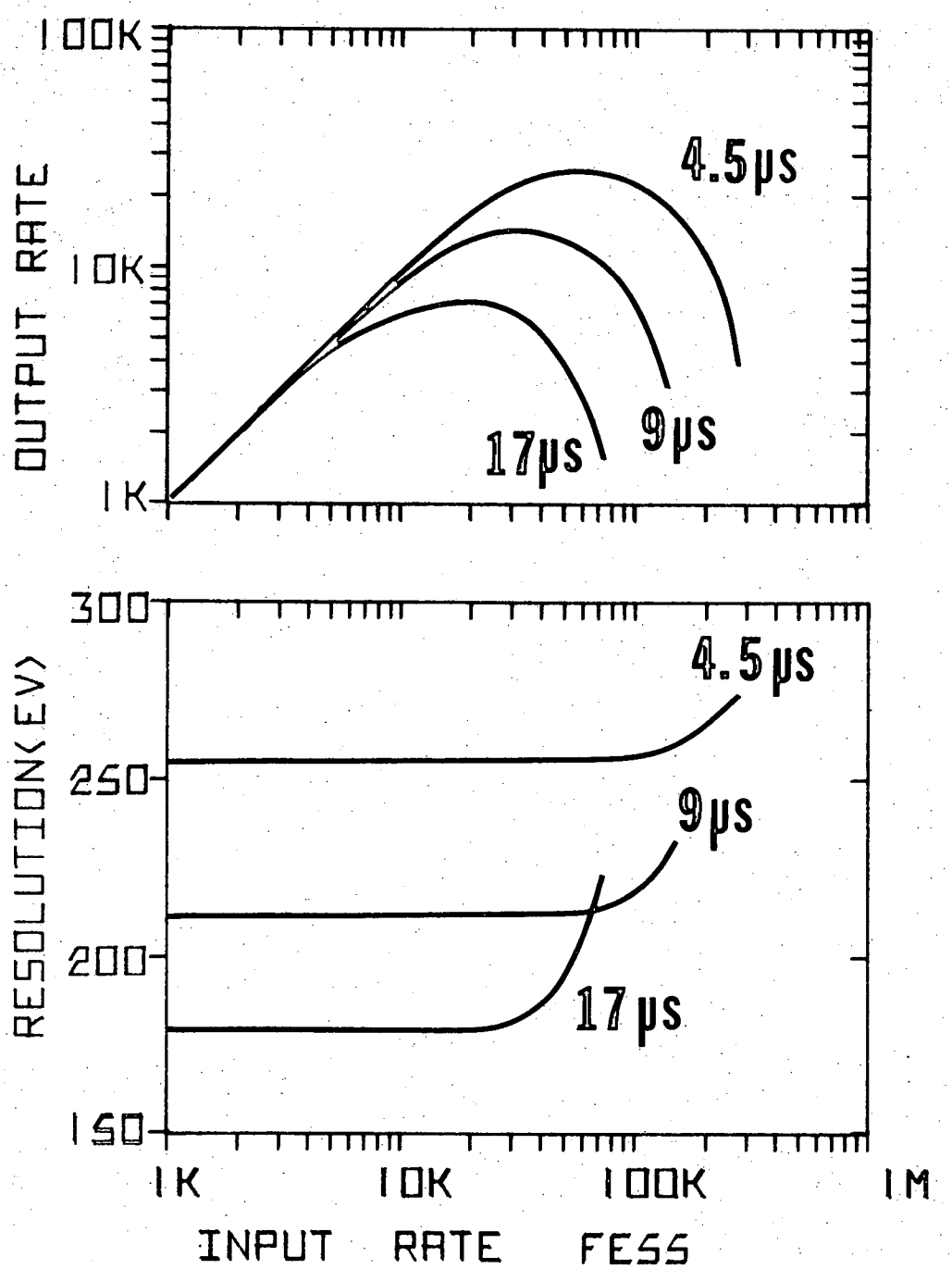

XBL 7010-6806

Fig. 14

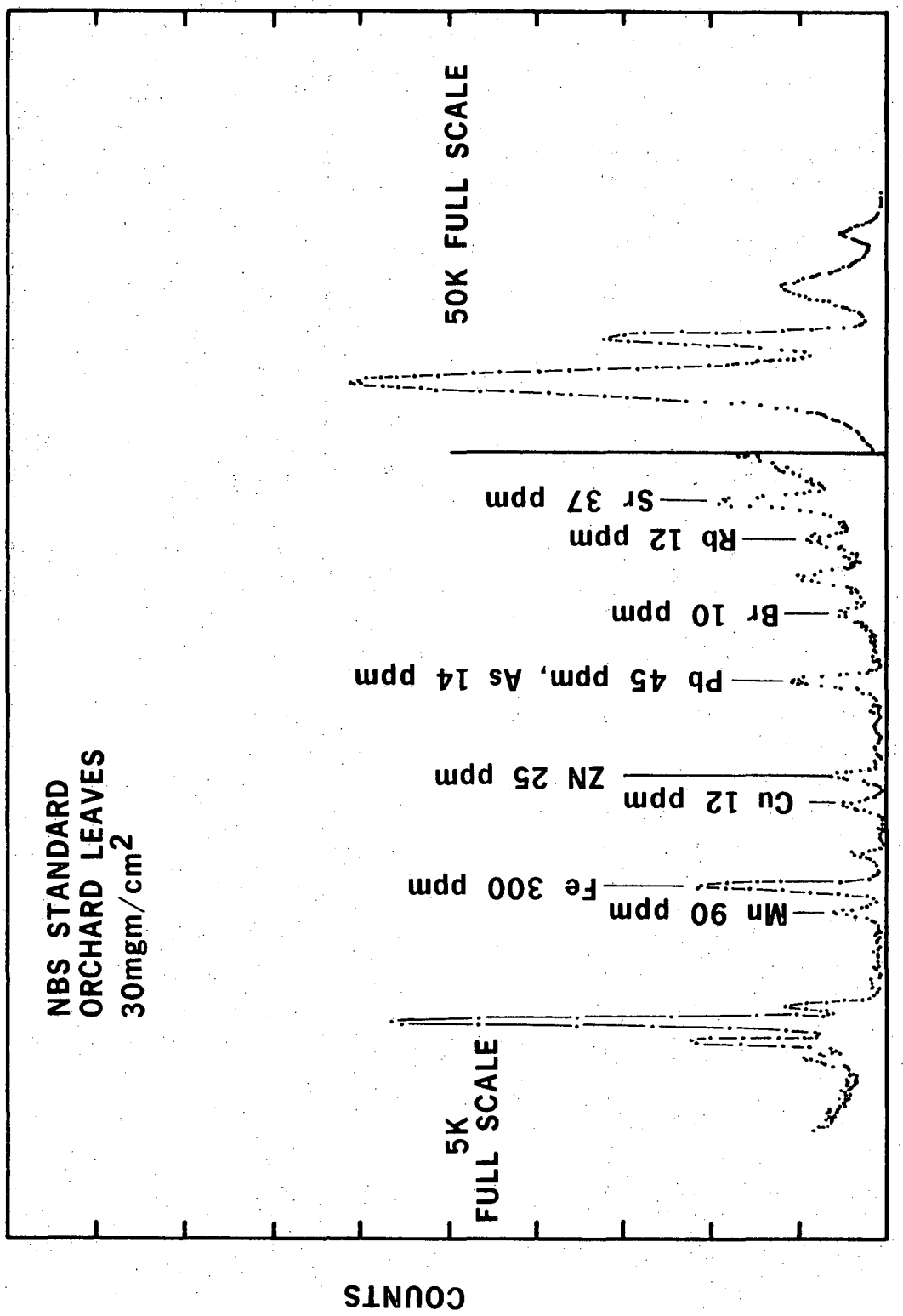
NBS STANDARD
ORCHARD LEAVES
30mgm/cm2
50K FULL SCALE
5K
FULL SCALE
Mn 90 ppm
Fe 300 ppm
Cu 12 ppm
ZN 25 ppm
Pb 45 ppm, As 14 ppm
Br 10 ppm
Rb 12 ppm
Sr 37 ppm
COUNTS
ENERGY
XBL 741-230

Fig. 15

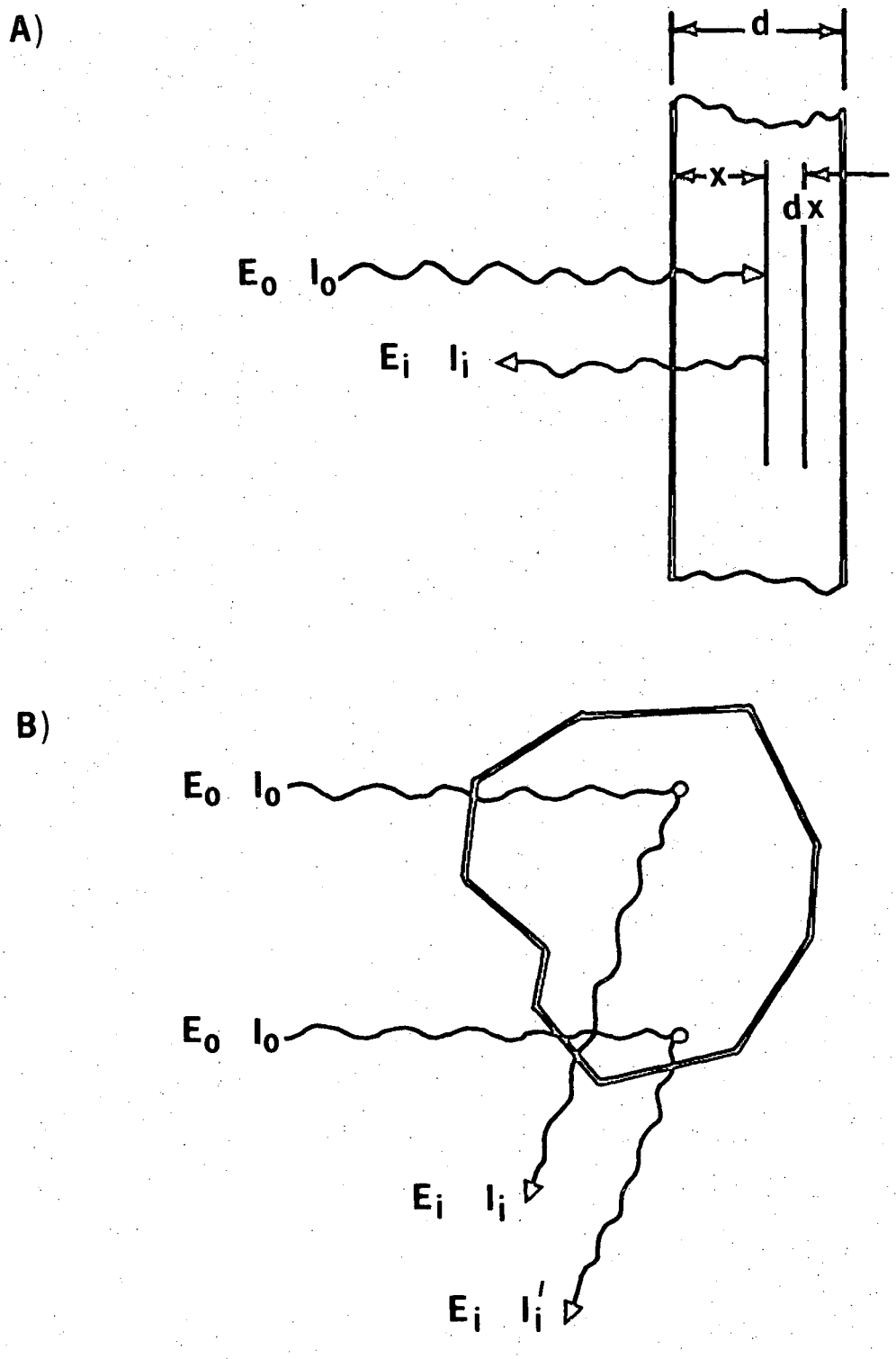

XBL 755-1349

Fig. 16 a) and b)

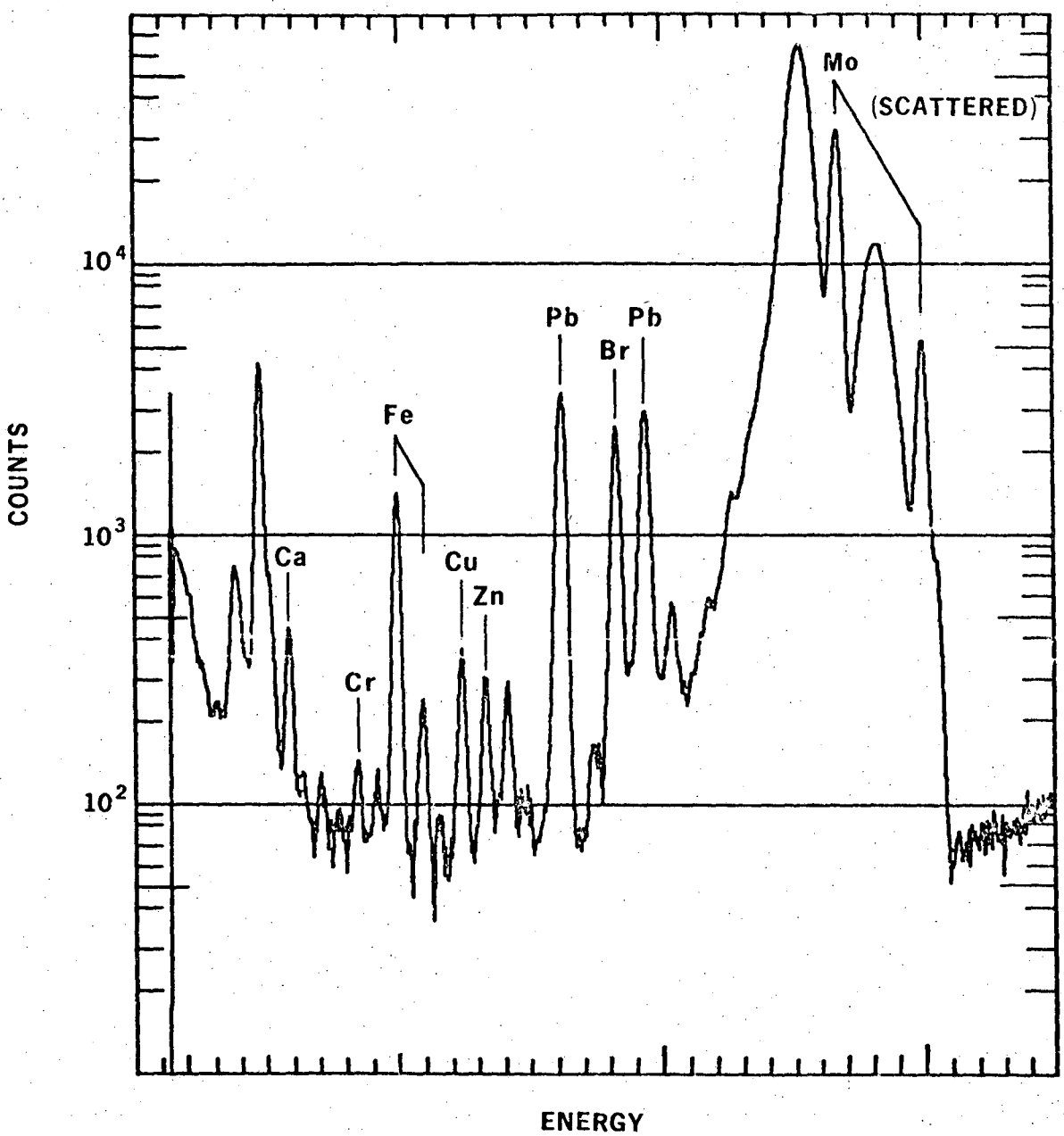

XBL 764-1601

Fig. 17

TECHNICAL INFORMATION DIVISION
LAWRENCE BERKELEY LABORATORY
UNIVERSITY OF CALIFORNIA
BERKELEY, CALIFORNIA 94720